Time evolution of entanglement entropy after quenches in two-dimensional free fermion systems: A dimensional reduction treatment

Shion Yamashika [1,2] Filiberto Ares [2] and Pasquale Calabrese [2,3]
[1]*Department of Physics, Chuo University, Bunkyo, Tokyo 112-8551, Japan*
[2]*SISSA and INFN, via Bonomea 265, 34136 Trieste, Italy*
[3]*International Centre for Theoretical Physics (ICTP), Strada Costiera 11, 34151 Trieste, Italy*

(Received 14 November 2023; revised 12 February 2024; accepted 22 February 2024; published 14 March 2024)

We study the time evolution of the Rényi entanglement entropies following a quantum quench in a two-dimensional (2D) free fermion system. By employing dimensional reduction, we effectively transform the 2D problem into decoupled chains, a technique applicable when the system exhibits translational invariance in one direction. Various initial configurations are examined, revealing that the behavior of entanglement entropies can often be explained by adapting the one-dimensional quasiparticle picture. However, intriguingly, for specific initial states the entanglement entropy saturates to a finite value without the reduced density matrix converging to a stationary state. We discuss the conditions necessary for a stationary state to exist and delve into the necessary modifications to the quasiparticle picture when such a state is absent.

DOI: 10.1103/PhysRevB.109.125122

I. INTRODUCTION

One of the most fundamental problems connecting quantum and statistical physics is how a statistical ensemble emerges in a closed many-body quantum system that evolves unitarily [1–3]. The common wisdom is that entanglement generates nonlocal correlations unique to quantum systems that spread throughout the system by unitary evolution: the resulting reduced density matrix for a local subsystem relaxes to a statistical ensemble such as the Gibbs ensemble [4–8] or, in the case of integrable systems, a generalized Gibbs ensemble (GGE) [9–15]. As a result, the expectation values of all the local observables in the subsystem coincide with those predicted by the corresponding statistical ensemble at large times. Given that the (von Neumann) entanglement entropy quantifies the amount of entanglement between the subsystem and the rest of the system [16–18], understanding its behavior in a unitary evolution is important to clarify how entanglement spreads and how thermodynamics arises in isolated quantum systems.

A popular and tractable setup to investigate the unitary evolution of a quantum many-body system is the quantum quench: the system is initially prepared in a nonequilibrium pure state $|\psi_0\rangle$ and then it is let to evolve in time with a postquench Hamiltonian H, $|\psi(t)\rangle = e^{-iH}|\psi_0\rangle$. In recent years, this protocol has been investigated not only theoretically but also experimentally thanks to remarkable developments in cold-atom and ion-trap systems [19–28].

The quench dynamics of the entanglement entropy in one-dimensional systems has been extensively studied in the literature. It has been found that it linearly increases in time and eventually saturates to a constant [29]; the latter can be identified with the thermodynamic entropy of the (generalized) Gibbs ensemble that describes locally the system at large times [30,31]. For integrable systems, this behavior is explained by the quasiparticle picture [29] in which the entanglement growth is due to the propagation of pairs of entangled quasiparticles. This picture has been validated for one-dimensional free [32–39] and interacting integrable systems [31,40–44] and generalized to different contexts [45–68] and quantities [69–92] (see also the reviews [93,94]). The same qualitative behavior for the time evolution of the entanglement entropy has been found in generic nonintegrable and chaotic interacting models with no quasiparticles (see, e.g., [95–102]). For many years, there has been a prevailing belief that the microscopic mechanism for the entanglement growth is fundamentally different in integrable and chaotic systems; only recently a unifying picture emerged in the space-time duality approach [86]. The Rényi entanglement entropies are a natural and important generalization of von Neumann one, not only because they help to calculate the former via the replica trick [103,104], but also because they carry further relevant information about the system and are measurable in cold-atom and ion-trap experiments [27,28,105–110]. While the quasiparticle picture captures the evolution of the Rényi entropies for free systems [32,42], it breaks down for interacting integrable models [86].

In higher dimensions $d \geqslant 2$, the entanglement entropy in equilibrium has been largely investigated (see, e.g., Refs. [111–130]); on the contrary its time evolution after a quantum quench has received little attention, mainly in field theory context [131–136]. For this reason, here we study the quench dynamics of Rényi entanglement entropies in a two-dimensional (2D) free fermion system. In particular, we apply a dimensional reduction approach, which was introduced in Ref. [137] and then has been applied to study, e.g., the (symmetry-resolved) entanglement entropy at equilibrium [126,129]. For a finite 2D system, periodic in both directions, this approach works as follows. The initial configuration

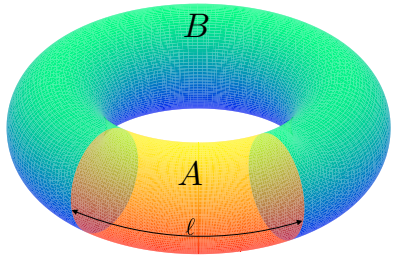

FIG. 1. Schematic representation of the two-dimensional system that we study and of the subsystem A considered.

should be translationally invariant (non-necessarily one-site shift invariant as we shall see) along one of the axes. Next we should choose as subsystem a periodic strip in this direction, as shown in Fig. 1. We can then decompose the Rényi entanglement entropies into the sum of the single-interval entanglement entropies of decoupled one-dimensional (1D) systems, for which exact results are known. We apply this strategy to calculate analytically the time evolution of the Rényi entanglement entropies for several particular initial configurations. We will see that our results can be explained in terms of a direct adaptation of the 1D quasiparticle picture, except for one particular initial configuration. The reason of such a mismatch is that the reduced density matrix does not attain a stationary value, even if its entanglement entropy does tend to a constant value. We then discuss the general conditions under which there is no stationary state in our 2D setting. From this observation, we deduce how the quasiparticle picture has to be modified to describe the behavior of the entropy in the absence of a stationary state.

The paper is organized as follows. In Sec. II, we introduce the setup and some basic quantities, including the Rényi entanglement entropy. In Sec. III, we describe the dimensional reduction approach. In Sec. IV, we apply it to obtain analytically the behavior of the entropies in quenches from several initial configurations. In Sec. V, we give a physical interpretation of the results obtained in the previous section in terms of the quasiparticle picture. In Sec. VI, we analyze the conditions for the existence of a stationary state and discuss how the quasiparticle picture modifies in that case. We finally draw our conclusions and present some outlooks in Sec. VII. We also include several Appendixes, where we derive some of the results presented in the main text.

II. SETUP AND SUMMARY OF RESULTS

We consider free fermions on a 2D square lattice with isotropic hopping between nearest-neighbor sites. The system is described by the Hamiltonian

$$H = -\frac{1}{2}\sum_{\langle \mathbf{i},\mathbf{i}'\rangle} a_{\mathbf{i}}^\dagger a_{\mathbf{i}'} + \text{H.c.}, \tag{1}$$

where $\mathbf{i} = (i_x, i_y)$ is a vector identifying a site of the lattice, $\langle \mathbf{i}, \mathbf{i}'\rangle$ stands for the nearest neighbors, and $a_{\mathbf{i}} = a_{i_x,i_y}$ ($a_{\mathbf{i}}^\dagger = a_{i_x,i_y}^\dagger$) is the annihilation (creation) operator of the fermion on the $\mathbf{i}$th site. We assume that the system size L_x (L_y) along the x (y) axis is even and that periodic boundary conditions are imposed along both directions.

Moving to Fourier modes

$$\tilde{a}_{\mathbf{q}} = \tilde{a}_{q_x,q_y} = \frac{1}{\sqrt{L_x L_y}}\sum_{\mathbf{i}} e^{-i\mathbf{q}\cdot\mathbf{i}} a_{\mathbf{i}}, \tag{2}$$

with quasimomenta $q_x = 0, 2\pi/L_x, \ldots, 2\pi(L_x-1)/L_x$ and $q_y = 0, 2\pi/L_y, \ldots, 2\pi(L_y-1)/L_y$, the Hamiltonian (1) is diagonalized as

$$H = \sum_{\mathbf{q}} \epsilon_{\mathbf{q}} \tilde{a}_{\mathbf{q}}^\dagger \tilde{a}_{\mathbf{q}}, \tag{3}$$

where the single-particle dispersion is $\epsilon_{\mathbf{q}} = -\cos q_x - \cos q_y$.

We consider the quantum quench described by the time-evolved state $|\psi(t)\rangle = e^{-itH}|\psi_0\rangle$ with an initial configuration $|\psi_0\rangle$ that is not an eigenstate of the Hamiltonian (1). We take as a subsystem A a periodic strip of length ℓ, as depicted in Fig. 1. That is, subsystem A is the set of sites $\mathbf{i}$ satisfying $i_x \in [0, \ell-1]$. The state of A is described by the reduced density matrix

$$\rho_A(t) = \text{Tr}_B(|\psi(t)\rangle\langle\psi(t)|), \tag{4}$$

where Tr_B denotes the trace over the subsystem B. The Rényi entanglement entropy,

$$S_n(\rho_A) = \frac{1}{1-n}\log \text{Tr}\big(\rho_A^n\big), \tag{5}$$

measures the degree of entanglement between subsystems A and B. In the limit $n \to 1$, it gives the von Neumann entanglement entropy,

$$S_1(\rho_A) = \lim_{n\to 1} S_n(\rho_A) = -\text{Tr}(\rho_A \log \rho_A). \tag{6}$$

Hereafter, we write $S_n(\rho_A)$ as S_n unless explicitly stated.

In this paper, we consider initial states $|\psi_0\rangle$ that satisfy Wick theorem. Therefore, since the postquench Hamiltonian is a quadratic fermionic operator, the time-evolved reduced density matrix $\rho_A(t)$ is Gaussian and it is fully characterized by the two-point correlation matrix restricted to subsystem A [138],

$$\Gamma_{\mathbf{i},\mathbf{i}'}(t) = 2\langle\psi(t)|\mathbf{a}_{\mathbf{i}}^\dagger \mathbf{a}_{\mathbf{i}'}|\psi(t)\rangle - \delta_{\mathbf{i},\mathbf{i}'}, \tag{7}$$

where $\mathbf{a}_{\mathbf{i}} = (a_{\mathbf{i}}^\dagger, a_{\mathbf{i}})$ and $\mathbf{i}, \mathbf{i}' \in A$. Γ is a matrix of dimension $2V_A \times 2V_A$, and V_A is the size of the subsystem A, $V_A = \ell L_y$. Using the standard algebra of Gaussian operators, the entanglement entropy can be expressed in terms of the two-point correlation matrix Γ as [33]

$$S_n = \frac{1}{2(1-n)}\text{Tr}\,\log\left[\left(\frac{I+\Gamma}{2}\right)^n + \left(\frac{I-\Gamma}{2}\right)^n\right], \tag{8}$$

where I is the $2V_A \times 2V_A$ identity matrix. For finite V_A, we can compute the trace in Eq. (8) and obtain the exact value of the entanglement entropy by numerically diagonalizing the two-point correlation matrix Γ. We will use this method as a benchmark of the analytic results obtained in the following sections.

To perform analytical calculations, it is useful to write the right-hand side of Eq. (8) as a Taylor series in the moments $\text{Tr}[\Gamma^m]$. To this end, we introduce the function $h_n(x)$:

$$h_n(x) = \frac{1}{1-n}\log\left[\left(\frac{1+x}{2}\right)^n + \left(\frac{1-x}{2}\right)^n\right]. \tag{9}$$

TABLE I. Summary of the particular initial states that we consider in Sec. IV and the corresponding time evolution of the Rényi entanglement entropy in the periodic strip of dimensions $\ell \times L_y$ of Fig. 1 after a quench to the Hamiltonian (1) in the ballistic regime $\ell, t \to \infty$ with t/ℓ fixed. The function $h_n(x)$ is defined in Eq. (9) and $v_x(q_x)$ is the quasiparticle velocity in the x direction, $v_x(q_x) = \partial_{q_x}\epsilon_{\mathbf{q}}$. A schematic representation of the initial configurations can be found in Fig. 2.

Initial state	Rényi entanglement entropy
Collinear Mott insulator state (Sec. IV A)	$S_n \simeq L_y \log(2) \int_0^{2\pi} \frac{\mathrm{d}q_x}{2\pi} \min(\ell, 2t\lvert v_x(q_x)\rvert)$
Mott insulator state (Sec. IV B)	$S_n \simeq L_y \log(2) \int_0^{2\pi} \frac{\mathrm{d}q_x}{2\pi} \min(\ell, 2t\lvert v_x(q_x)\rvert)$
Collinear dimer state (Sec. IV C)	$S_n \simeq L_y \int_0^{2\pi} \frac{\mathrm{d}q_x}{2\pi} h_n(\cos q_x) \min(\ell, 2t\lvert v_x(q_x)\rvert)$
Staggered dimer state (Sec. IV D)	$S_n \simeq L_y \int_0^{2\pi} \frac{\mathrm{d}q_x}{2\pi} h_n(\cos q_x) \min(\ell, 2t\lvert v_x(q_x)\rvert)$
Diagonal dimer state (Sec. IV E)	$S_n \simeq \sum_{q_y} \int_0^{2\pi} \frac{\mathrm{d}q_x}{2\pi} h_n[\cos(q_x + q_y)] \min(\ell, 2t\lvert v_x(q_x)\rvert)$
Crossed dimer state (Sec. IV F)	$S_n = L_y \int_0^{2\pi} \frac{\mathrm{d}q_x}{2\pi} h_n(\cos q_x) \min(\ell, 2t\lvert v_x(q_x)\rvert)$
Partially filled product state I (Sec. IV G 1)	$S_n \simeq L_y \int_0^{2\pi} \frac{\mathrm{d}q_x}{2\pi} h_n(\cos \Delta_{q_x}) \min(\ell, 2t\lvert v_x(q_x)\rvert)$
Partially filled product state II (Sec. IV G 2)	$S_n \simeq \sum_{q_y} h_n(\cos \Delta_{q_y}) \int_0^{2\pi} \frac{\mathrm{d}q_x}{2\pi} \min(\ell, 2t\lvert v_x(q_x)\rvert)$

This function can be expanded as

$$h_n(x) = \sum_{m=0}^{\infty} a_n(2m) x^{2m}, \tag{10}$$

and, therefore, Eq. (8) can be rewritten in the form

$$S_n = \frac{1}{2} \sum_{m=0}^{\infty} a_n(2m) \mathrm{Tr}(\Gamma^{2m}). \tag{11}$$

As we will see in the next sections, the precise form of the coefficients $a_n(2m)$ is never needed and hence will not be reported.

In what follows, we will study the Rényi entanglement entropies in a periodic strip after a quench to the Hamiltonian (1) from the initial Gaussian configurations of Table I. In that table, we report the exact analytic expressions that we obtain for the entanglement entropy in each quench in the ballistic regime $t, \ell \to \infty$ with t/ℓ fixed. In Sec. III, we describe the dimensional reduction method that we apply in Sec. IV to derive these results. In Secs. V and VI, we discuss their physical interpretation in terms of the quasiparticle picture.

III. DIMENSIONAL REDUCTION

In this section, we present the dimensional reduction approach that we will employ in Sec. IV to calculate analytically the time evolution of the Rényi entanglement entropy in different quantum quenches. The treatment is generically valid for initial states $|\psi_0\rangle$ that are invariant under k-site translations in the y direction, with k being a factor of L_y. For clarity, we present first the case $k = 1$ and after we generalize straightforwardly to arbitrary k.

A. One-site shift-invariant states in the transverse direction

We start considering the case when the initial state $|\psi_0\rangle$ is translationally invariant in the y direction. Since the Hamiltonian (1) preserves the translational symmetry, the time-evolved state $|\psi(t)\rangle$ is also invariant.

Given the geometry of the subsystem A considered, it is useful to take the Fourier transform only along the y direction by introducing the fermionic operators in a mixed space-momentum basis

$$c_{i_x,q_y} = \frac{1}{\sqrt{L_y}} \sum_{i_y} e^{-\mathrm{i}q_y i_y} a_{i_x,i_y}, \tag{12}$$

which is the core of the dimensional reduction method. The two-point correlation function Γ can be written as

$$\Gamma_{(i_x,j_y),(i'_x,j'_y)} = \frac{1}{L_y} \sum_{n_y=0}^{L_y-1} e^{\mathrm{i}\frac{2\pi n_y}{L_y}(j_y - j'_y)} (\Gamma_{q_y})_{i_x,i'_x}, \tag{13}$$

where Γ_{q_y} is the $2\ell \times 2\ell$ two-point correlation matrix in the mixed space-momentum representation and the sum of $q_y = 2\pi n_y/L_y$ runs on the L_y allowed transverse modes. As a consequence, modulo the Fourier transform which is a unitary operation, we have the decomposition

$$\Gamma \simeq \bigoplus_{n_y=0}^{L_y-1} \Gamma_{q_y}, \tag{14}$$

and so the entanglement entropy admits the decomposition in L_y-independent terms

$$S_n = \sum_{n_y=0}^{L_y-1} S_n(\Gamma_{q_y}), \tag{15}$$

where we denoted by $S_n(\Gamma_{q_y})$ the Rényi entropy of the Gaussian state of a 1D chain with correlation matrix Γ_{q_y}. Notice that the decomposition (15) is valid for arbitrary values of L_x and L_y, not necessarily in the thermodynamic limit.

B. k-site shift-invariant states in the transverse direction

Let us now assume that the initial state $|\psi_0\rangle$ is invariant under k-site translations in the y direction with k being a factor of L_y. Once again, since the Hamiltonian (1) preserves the translational symmetry, the time-evolved state $|\psi(t)\rangle$ is also invariant under k-site translations. This property is inherited by the two-point correlation matrix $\Gamma(t)$ (7), and its entries satisfy

$$\Gamma_{(i_x,i_y+mk),(i'_x,i'_y+mk)} = \Gamma_{(i_x,i_y),(i'_x,i'_y)}, \quad \forall\, m \in \mathbb{Z}. \tag{16}$$

Therefore, it is convenient to decompose the index in the y direction as $i_y = kj_y + p$, with $j_y = 0, \ldots, L_y/k - 1$ and $p = 0, \ldots, k-1$, and then rearrange the entries of $\Gamma(t)$ in $k \times k$ blocks of the form

$$\Gamma_{(i_x,j_y),(i'_x,j'_y)}(t) = 2\langle\psi(t)|\vec{\mathbf{a}}^\dagger_{i_x,j_y}\vec{\mathbf{a}}_{i'_x,j'_y}|\psi(t)\rangle - \delta_{i_x,i'_x}\delta_{j_y,j'_y}, \tag{17}$$

where $\vec{\mathbf{a}}_{i_x,j_y} = (\mathbf{a}_{i_x,kj_y}, \mathbf{a}_{i_x,kj_y+1}, \ldots, \mathbf{a}_{i_x,kj_y+k-1})$, with $i_x \in A$.

Once again, we take the Fourier transform only along the y direction using Eq. (12). The two-point correlation function Γ can be then written as

$$\Gamma_{(i_x,j_y),(i'_x,j'_y)} = \frac{k}{L_y}\sum_{n_y=0}^{\frac{L_y}{k}-1} e^{\mathrm{i}\frac{2\pi k n_y}{L_y}(j_y-j'_y)}(\mathcal{G}^{(k)}_{q_y})_{i_x,i'_x}, \tag{18}$$

where

$$\left(\mathcal{G}^{(k)}_{q_y}\right)_{i_x,i'_x} = U\left(\Gamma^{(k)}_{q_y}\right)_{i_x,i'_x}U^\dagger. \tag{19}$$

Here U is a unitary matrix with entries $U_{pp'} = e^{\mathrm{i}2\pi\left(\frac{p}{L_y}+\frac{pp'}{k}\right)}/\sqrt{k}$ and $(\Gamma^{(k)}_{q_y})_{i_x,i'_x}$ is the $2k\ell \times 2k\ell$ two-point correlation matrix in the mixed space-momentum representation whose entries are rearranged in $k \times k$ blocks as

$$\left(\Gamma^{(k)}_{q_y}\right)_{i_x,i'_x} = 2\langle\psi(t)|\vec{\mathbf{c}}^\dagger_{i_x,q_y}\vec{\mathbf{c}}_{i'_x,q_y}|\psi(t)\rangle - \delta_{i_x,i'_x}, \tag{20}$$

where $q_y = \frac{2\pi n_y}{L_y}$ and

$$\vec{\mathbf{c}}_{i_x,q_y} = \left(\mathbf{c}_{i_x,q_y}\ \mathbf{c}_{i_x,q_y+\frac{2\pi}{k}}\ldots\mathbf{c}_{i_x,q_y+\frac{2\pi(k-1)}{k}}\right) \tag{21}$$

with $\mathbf{c}_{i_x,q_y} = (c^\dagger_{i_x,q_y}, c_{i_x,-q_y})$.

Given Eq. (18), the matrix Γ takes the form

$$\Gamma = \frac{k}{L_y}\sum_{n_y=0}^{\frac{L_y}{k}-1}\mathcal{G}^{(k)}_{q_y}\otimes T_{q_y}, \tag{22}$$

where we have introduced the matrices $(T_{q_y})_{j_yj'_y} = e^{\mathrm{i}kq_y(j_y-j'_y)}$. These matrices mutually commute and can be diagonalized simultaneously by

$$V_{j_y,j'_y} = \frac{1}{\sqrt{k}}e^{\mathrm{i}2\pi\, j_y j'_y/k} \tag{23}$$

such that $(VT_{q_y}V^\dagger)_{j_y,j'_y} = k\delta_{q_y,j_y}\delta_{q_y,j'_y}$. As a consequence, we have the decomposition

$$(I\otimes V)\Gamma(I\otimes V^\dagger) = \bigoplus_{n_y=0}^{\frac{L_y}{k}-1}\mathcal{G}^{(k)}_{q_y}, \tag{24}$$

showing that the two-point correlation matrix Γ is block diagonal in the q_y transverse momentum sectors. Plugging Eq. (24) into Eq. (8), and taking into account that $\mathcal{G}^{(k)}_{q_y}$ and $(\Gamma^{(k)}_{q_y})$ are related by a unitary transformation (19), we finally obtain

$$S_n = \sum_{n_y=0}^{\frac{L_y}{k}-1} S_n\left(\Gamma^{(k)}_{q_y}\right) = \frac{1}{2}\sum_{n_y=0}^{\frac{L_y}{k}-1}\sum_{m=0}^{\infty} a_n(2m)\mathrm{Tr}\left[\left(\Gamma^{(k)}_{q_y}\right)^{2m}\right]. \tag{25}$$

Accordingly, the entanglement entropy in our 2D system is the sum of the single-interval entanglement entropies of L_y/k one-dimensional fermionic chains, each univocally characterized by the correlation matrices $\Gamma^{(k)}_{q_y}$.

IV. EXAMPLES

In this section, using the dimensional reduction approach described in Sec. III and invoking results for 1D systems, we calculate the entanglement entropy in quantum quenches from several initial states. In particular, we analytically derive its exact behavior in the ballistic regime in which $t, \ell \to \infty$ with t/ℓ fixed, taking the thermodynamic limit in the longitudinal direction $L_x \to \infty$, with the transverse one L_y finite. Here, we only present the results of the calculations, while their physical interpretation will be discussed in Sec. V.

For the concrete initial configurations that we will consider, the time evolution of the entanglement entropy can be calculated using Eq. (25). The latter requires the knowledge of the matrix $\Gamma^{(k)}_{q_y}$ defined in Eq. (20), which involves the mixed space-momentum correlations $\langle c^\dagger_{i_x,q_y}c_{i'_x,q'_y}\rangle$ and $\langle c_{i_x,q_y}c_{i'_x,q'_y}\rangle$. Their time evolution can be easily computed employing the Heisenberg picture since the momentum modes $\tilde{a}_{\mathbf{q}}$ that diagonalize the postquench Hamiltonian (1) evolve trivially in time as $\tilde{a}_{\mathbf{q}}(t) = e^{-\mathrm{i}t\epsilon_{\mathbf{q}}}\tilde{a}_{\mathbf{q}}$. Therefore, taking the partial Fourier transform in the x direction, we have

$$\begin{aligned}&\langle\psi(t)|c^\dagger_{i_x,q_y}c_{i'_x,q'_y}|\psi(t)\rangle\\ &\quad= \frac{1}{L_x}\sum_{q_x,q'_x} e^{-\mathrm{i}(q_xi_x-q'_xi'_x)}e^{\mathrm{i}t(\epsilon_{\mathbf{q}}-\epsilon_{\mathbf{q}'})}\langle\psi_0|\tilde{a}^\dagger_{\mathbf{q}}\tilde{a}_{\mathbf{q}'}|\psi_0\rangle\end{aligned} \tag{26}$$

and

$$\begin{aligned}&\langle\psi(t)|c_{i_x,q_y}c_{i'_x,q'_y}|\psi(t)\rangle\\ &\quad= \frac{1}{L_x}\sum_{q_x,q'_x} e^{\mathrm{i}(q_xi_x+q'_xi'_x)}e^{-\mathrm{i}t(\epsilon_{\mathbf{q}}+\epsilon_{\mathbf{q}'})}\langle\psi_0|\tilde{a}_{\mathbf{q}}\tilde{a}_{\mathbf{q}'}|\psi_0\rangle.\end{aligned} \tag{27}$$

Writing now the operators $\tilde{a}_{\mathbf{q}}$ and $\tilde{a}^\dagger_{\mathbf{q}}$ in terms of the real space ones $a_{\mathbf{i}}$ and $a^\dagger_{\mathbf{i}}$, we find

$$\begin{aligned}\langle\psi(t)|c^\dagger_{i_x,q_y}c_{i'_x,q'_y}|\psi(t)\rangle = \frac{1}{L_x^2L_y}&\sum_{q_x,q'_x}\sum_{\mathbf{j},\mathbf{j}'} e^{-\mathrm{i}(q_xi_x-q'_xi'_x)}\\ &\times e^{\mathrm{i}t(\epsilon_{\mathbf{q}}-\epsilon_{\mathbf{q}'})}e^{\mathrm{i}(\mathbf{q}\cdot\mathbf{j}-\mathbf{q}'\cdot\mathbf{j}')}\langle\psi_0|a^\dagger_{\mathbf{j}}a_{\mathbf{j}'}|\psi_0\rangle\end{aligned} \tag{28}$$

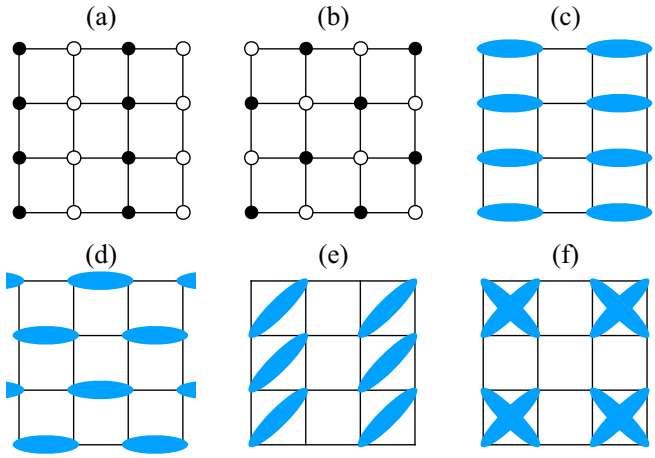

FIG. 2. Schematic representations of the states that we consider as initial configurations for the quantum quenches. They are (a) the collinear Mott state, (b) the Mott state, (c) the collinear dimer state, (d) the staggered dimer state, (e) the diagonal dimer state, and (f) the crossed dimer state. The black and white dots represent the occupied and empty sites, respectively. The blue ellipses represent singlet pairs.

and

$$\langle\psi(t)|c_{i_x,q_y}c_{i'_x,q'_y}|\psi(t)\rangle = \frac{1}{L_x^2 L_y}\sum_{q_x,q'_x}\sum_{\mathbf{j},\mathbf{j}'} e^{\mathrm{i}(q_x i_x + q'_x i'_x)} \times e^{-\mathrm{i}t(\epsilon_{\mathbf{q}}+\epsilon_{\mathbf{q}'})} e^{-\mathrm{i}(\mathbf{q}\cdot\mathbf{j}-\mathbf{q}'\cdot\mathbf{j}')}\langle\psi_0|a_{\mathbf{j}}a_{\mathbf{j}'}|\psi_0\rangle. \quad (29)$$

Equations (28) and (29) recast the time evolution of the correlators $\langle c^\dagger_{i_x,q_y}c_{i'_x,q'_y}\rangle$, $\langle c_{i_x,q_y}c_{i'_x,q'_y}\rangle$, and, consequently of the matrix $\Gamma^{(k)}_{q_y}$, in terms of the $t=0$ correlators $\langle a^\dagger_{\mathbf{j}}a_{\mathbf{j}'}\rangle$ and $\langle a_{\mathbf{j}}a_{\mathbf{j}'}\rangle$.

A. Collinear Mott insulator state

We start with the quantum quench from the collinear Mott insulator state, which is defined as

$$|\mathrm{CM}\rangle = \prod_{i_x=0}^{\frac{L_x}{2}-1}\prod_{i_y=0}^{L_y-1} a^\dagger_{2i_x,i_y}|0\rangle, \quad (30)$$

where $|0\rangle$ is the space vacuum state; i.e., $a_{\mathbf{i}}|0\rangle = 0$ for all $\mathbf{i}$. We schematically represent this configuration in Fig. 2(a). The collinear Mott insulator state (30) is a product state and, therefore, the entanglement entropy for any bipartition is zero.

According to Eq. (25), since the state (30) is invariant under single-site translations in the y direction, the entanglement entropy after the quench can be calculated from the correlation matrix $\Gamma^{(1)}_{q_y}$. The entries of this matrix [see Eq. (20)] are given by the correlators $\langle c^\dagger_{i_x,q_y}c_{i'_x,q'_y}\rangle$ and $\langle c_{i_x,q_y}c_{i'_x,q'_y}\rangle$, whose time evolution can be obtained with Eqs. (28) and (29) in terms of $\langle a^\dagger_{\mathbf{j}}a_{\mathbf{j}'}\rangle$ and $\langle a_{\mathbf{j}}a_{\mathbf{j}'}\rangle$ for the initial state, which in this case read as

$$\langle\mathrm{CM}|a^\dagger_{\mathbf{j}}a_{\mathbf{j}'}|\mathrm{CM}\rangle = \frac{\delta_{\mathbf{j},\mathbf{j}'}}{2}[1+(-1)^{j_x}] \quad (31)$$

and

$$\langle\mathrm{CM}|a_{\mathbf{j}}a_{\mathbf{j}'}|\mathrm{CM}\rangle = 0. \quad (32)$$

Note that the pairing correlation functions such as $\langle c_{i_x,q_y}c_{i'_x,-q_y}\rangle$ vanish because the state (30) has a definite number of excitations.

Plugging Eqs. (31) and (32) in (28) and (29), respectively, we obtain

$$(\Gamma^{(1)}_{q_y})_{i_x,i'_x}(t) = \begin{pmatrix} -C_{i'_x,i_x}(t) & 0 \\ 0 & C_{i_x,i'_x}(t)\end{pmatrix}, \quad (33)$$

where $C_{i_x,i'_x}(t)$ is the 1D correlation matrix after the quench to the tight-binding fermionic chain from the Néel state (see, e.g., [80]). In the thermodynamic limit $L_x\to\infty$, it reads as

$$C_{i_x,i'_x}(t) = (-1)^{i'_x}\int_0^{2\pi}\frac{\mathrm{d}q_x}{2\pi}e^{-\mathrm{i}q_x(i_x-i'_x)-2\mathrm{i}t\cos q_x}. \quad (34)$$

Plugging Eq. (33) into (25) with $k=1$, we obtain

$$S_n = \sum_{n_y=0}^{L_y-1} S_n(C) = L_y S_n(C). \quad (35)$$

The asymptotic form of the 1D entanglement entropy with correlation matrix (34) in the ballistic regime is known [80]

$$S_n(C) \simeq \log(2)\int_0^{2\pi}\frac{\mathrm{d}q_x}{2\pi}\min(\ell, 2t|v_x(q_x)|), \quad (36)$$

where $v_x(q_x) = \partial_{q_x}\epsilon_{\mathbf{q}} = \sin q_x$ is the fermion velocity in the x direction and, by $\simeq$, we always mean equal in the thermodynamic and ballistic limits. Hence, for the 2D model we obtain that

$$S_n(t) \simeq L_y\log(2)\int_0^{2\pi}\frac{\mathrm{d}q_x}{2\pi}\min(\ell, 2t|v_x(q_x)|). \quad (37)$$

The expression above shows that the entanglement entropy linearly increases in time for $t < \ell/\max(2v_x) = \ell/2$, while for $t \gg \ell/2$ it saturates to a constant value

$$\lim_{t\to\infty} S_n \simeq V_A\log(2). \quad (38)$$

In Fig. 3, we report the time evolution of the entanglement entropy for the quench from the collinear Mott insulator state. The curve is the analytic result (37), which agrees well with the exact numerical data obtained using Eq. (8).

B. Mott insulator state

We now consider the quantum quench from the Mott insulator state, which is defined as

$$|\mathrm{M}\rangle = \prod_{i_x+i_y=\mathrm{even}} a^\dagger_{\mathbf{i}}|0\rangle. \quad (39)$$

This state is represented schematically in Fig. 2(b). As in the case of the collinear Mott insulator state discussed in Sec. IV A, this configuration is also a product state and, therefore, the entanglement entropy at $t=0$ is zero.

Since the Mott insulator state is invariant under two-site translations in the y direction, the entanglement entropy after the quench can be obtained by applying Eq. (25) once we have determined the time evolution of the correlation matrix $\Gamma^{(2)}_{q_y}$.

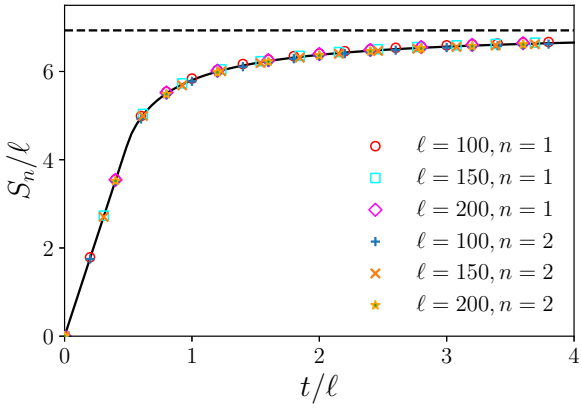

FIG. 3. Time evolution of the Rényi entanglement entropy in the quantum quench from the collinear Mott insulator and Mott insulator states. The solid line is the analytic result in Eq. (37). The symbols are the exact value of the entropy obtained numerically using Eq. (8). We take $L_y = 10$.

Using Eqs. (28) and (29), we only need the two-point spatial correlations in the initial configuration to calculate it. For the Mott insulator state,

$$\langle \mathrm{M}|a^\dagger_{\mathbf{j}} a_{\mathbf{j}'}|\mathrm{M}\rangle = \frac{\delta_{\mathbf{j},\mathbf{j}'}}{2}[1+(-1)^{j_x+j_y}] \tag{40}$$

and

$$\langle \mathrm{M}|a_{\mathbf{j}} a_{\mathbf{j}'}|\mathrm{M}\rangle = 0. \tag{41}$$

If we insert them in Eqs. (28) and (29), respectively, we obtain that the matrix $\Gamma^{(2)}_{q_y}$ is

$$\begin{aligned}\left(\Gamma^{(2)}_{q_y}\right)_{i_x,i'_x}(t) = U e^{\mathrm{i}t\cos q_y \sigma_z\otimes\sigma_z} \\ \times \begin{pmatrix} -C_{i'_x,i_x}(t) & 0 \\ 0 & C_{i_x,i'_x}(t)\end{pmatrix}\otimes\sigma_x \\ \times\ e^{-\mathrm{i}t\cos q_y\sigma_z\otimes\sigma_z}U^{-1},\end{aligned} \tag{42}$$

where the matrix C is the same as in Eq. (33), σ_μ are the Pauli matrices, and $U = I/2 + \sum_{\mu=x,y,z}\sigma_\mu\otimes\sigma_\mu/2$. In the thermodynamic limit $L_x\to\infty$, C is given by Eq. (34). Plugging this result into Eq. (25) with $k=2$ and using $\mathrm{Tr}\sigma_x^{2m} = 2$, we obtain

$$S_n = L_y S_n(C), \tag{43}$$

which coincides with the expression found in Eq. (35) for the collinear Mott insulator state (30). The matrix C is the same in the Mott insulator and in the collinear Mott insulator states, both at finite size L_x and when we take $L_x\to\infty$, and therefore the entanglement entropy presents exactly the same time evolution in both quenches and for this reason we do not report any numerical test.

C. Collinear dimer state

Let us now analyze the quantum quench from the collinear dimer state,

$$|\mathrm{CD}\rangle = \prod_{i_x=0}^{\frac{L_x}{2}-1}\prod_{i_y=0}^{L_y-1}\frac{a^\dagger_{2i_x,i_y} - a^\dagger_{2i_x+1,i_y}}{\sqrt{2}}|0\rangle, \tag{44}$$

which is represented in Fig. 2(c). Unlike the previous examples, this configuration is not a product state for each site, but the $(2i_x, i_y)$th and $(2i_x+1, i_y)$th pairs of sites are entangled by the singlet pairing. However, since these singlet pairs do not cross the boundaries of the subsystem considered (because we choose ℓ to be even and its end points to be also end points of singlets), we have that the entanglement entropy is zero before the quench.

The collinear dimer state (44) has one-site translational symmetry in the y direction. Since it is invariant under two-site translations in the x direction, it is convenient to rearrange the entries of the correlation matrix $\Gamma^{(1)}_{q_y}$, which enters in the computation of the entropy (25), as

$$\left(\Gamma^{(1)}_{q_y}\right)_{i_x,i'_x} = 2\left\langle\begin{pmatrix}\mathbf{c}^\dagger_{2i_x,q_y}\\ \mathbf{c}^\dagger_{2i_x+1,q_y}\end{pmatrix}(\mathbf{c}_{2i'_x,q_y}\ \mathbf{c}_{2i'_x+1,q_y})\right\rangle - \delta_{i_x,i'_x}I_4, \tag{45}$$

with $i_x, i'_x \in [0, \ell/2-1]$. The correlators in $\Gamma^{(1)}_{q_y}$ can be calculated using Eqs. (28) and (29) with

$$\langle \mathrm{CD}|a^\dagger_{\mathbf{j}}a_{\mathbf{j}'}|\mathrm{CD}\rangle = \frac{1}{2}\delta_{\mathbf{j},\mathbf{j}'} - \frac{1}{4}\delta_{j_y,j'_y}\delta_{j_x\pm1,j'_x} \pm \frac{(-1)^{j_x}}{4}\delta_{j_y,j'_y}\delta_{j_x\pm1,j'_x}$$

and

$$\langle \mathrm{CD}|a_{\mathbf{j}}a_{\mathbf{j}'}|\mathrm{CD}\rangle = 0. \tag{46}$$

In this way, once we have properly organized all the entries of $\Gamma^{(1)}_{q_y}$, we find that it takes the form

$$\left(\Gamma^{(1)}_{q_y}\right)_{i_x,i'_x} = U\begin{pmatrix}-T^{\mathrm{D}}_{i'_x,i_x} & 0\\ 0 & T^{\mathrm{D}}_{i_x,i'_x}\end{pmatrix}U^\dagger, \tag{47}$$

where $U = I_4/2 + \sum_{\mu=x,y,z}\sigma_\mu\otimes\sigma_\mu/2$ is a 4×4 unitary matrix and T^{D} is equal to the 1D two-point correlation matrix of the quench to the tight-binding fermionic chain from the dimer state (see, e.g., Ref. [80]). In the thermodynamic limit $L_x\to\infty$, T^{D} is a block Toeplitz matrix

$$T^{\mathrm{D}}_{i_x,i'_x} = \int_0^{2\pi}\frac{\mathrm{d}q_x}{2\pi}e^{-2\mathrm{i}q_x(i_x-i'_x)}g_{\mathrm{D}}(q_x), \tag{48}$$

generated by the 2×2 symbol $g_{\mathrm{D}}(q_x)$,

$$g_{\mathrm{D}}(q_x) = e^{\mathrm{i}\sigma_z\frac{q_x}{2}}(\sigma_-\sin q_x e^{-2\mathrm{i}t\cos q_x} - \sigma_x\cos q_x)e^{-\mathrm{i}\sigma_z\frac{q_x}{2}}, \tag{49}$$

with $\sigma_\pm = \sigma_y \pm \mathrm{i}\sigma_z$.

Plugging Eq. (47) into (25), we obtain

$$S_n = L_y S_n(T^{\mathrm{D}}). \tag{50}$$

In the ballistic regime, the asymptotic form of entropy $S_n(T^{\mathrm{D}})$ is known and reads as [80]

$$S_n(T^{\mathrm{D}}) \simeq \int_0^{2\pi}\frac{\mathrm{d}q_x}{2\pi}h_n(\cos q_x)\min(\ell, 2t|v_x(q_x)|), \tag{51}$$

providing that the Rényi entanglement entropy after the quench in 2D behaves as

$$S_n \simeq L_y\int_0^{2\pi}\frac{\mathrm{d}q_x}{2\pi}h_n(\cos q_x)\min(\ell, 2t|v_x(q_x)|). \tag{52}$$

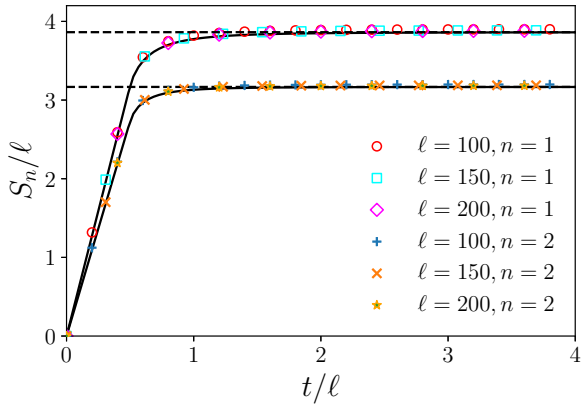

FIG. 4. Rényi entanglement entropy as a function of t/ℓ in a quench from the collinear dimer state for $n \to 1$ and $n = 2$ and different subsystem lengths ℓ. The solid lines correspond to the analytic prediction obtained in Eq. (52). The dashed lines indicate the saturation value (53). The symbols are the exact numerical value of the entropies calculated employing Eq. (8). We take $L_y = 10$.

Therefore, the entanglement entropy increases linearly in time for $t < \ell/2$, while it approaches the constant value

$$\lim_{t\to\infty} S_n \simeq V_A \int_0^{2\pi} \frac{\mathrm{d}q_x}{2\pi} h_n(\cos q_x) \tag{53}$$

at large times $t \gg \ell/2$.

In Fig. 4, we check the validity of the analytic result (52). We plot it for $n \to 1$ and $n = 2$, as a function of time (solid curves) and we compare with the exact numerical value computed using Eq. (8).

D. Staggered dimer state

We now investigate a modification of the previous initial configuration, the staggered dimer state, which is defined as

$$|\mathrm{SD}\rangle = \prod_{i_x+i_y=\text{even}} \frac{a^\dagger_{i_x,i_y} - a^\dagger_{i_x+1,i_y}}{\sqrt{2}}|0\rangle \tag{54}$$

and illustrated in Fig. 2(d). In this case, there are L_y singlet pairs crossing the boundary of the subsystem and, consequently, the initial entanglement entropy is $S_n = L_y \log(2)$ at $t = 0$. This initial offset is subleading (and hence negligible) in the ballistic limit because it does not scale with the volume $V_A = \ell L_y$.

The staggered dimer state (54) is invariant under two-site translations in the y direction, i.e., $k = 2$. Since it is also invariant under two-site translations in the x direction, it is convenient to rearrange the entries of the matrix $\Gamma^{(2)}_{q_y}$ as

$$\left(\Gamma^{(2)}_{q_y}\right)_{i_x,i'_x} = 2\left\langle \begin{pmatrix} \vec{\mathbf{c}}^\dagger_{2i_x,q_y} \\ \vec{\mathbf{c}}^\dagger_{2i_x+1,q_y} \end{pmatrix} \left(\vec{\mathbf{c}}_{2i'_x,q_y}\ \vec{\mathbf{c}}_{2i'_x+1,q_y}\right) \right\rangle - \delta_{i_x,i'_x} I_8, \tag{55}$$

with $i_x, i'_x \in [0, \ell/2-1]$. The definition of $\vec{\mathbf{c}}_{i_x,q_y}$ is given in Eq. (21). The entries of $\Gamma^{(2)}_{q_y}$ can be calculated by plugging the initial state correlators

$$\langle \mathrm{SD}|a^\dagger_{\mathbf{j}} a_{\mathbf{j}'}|\mathrm{SD}\rangle = \frac{\delta_{\mathbf{j},\mathbf{j}'}}{2} - \frac{1}{4}\delta_{j_y,j'_y}\delta_{j_x\pm1,j'_x} \pm \frac{(-1)^{j_x+j_y}}{4}\delta_{j_y,j'_y}\delta_{j_x\pm1,j_x}, \tag{56}$$

and $\langle \mathrm{SD}|a_{\mathbf{j}} a_{\mathbf{j}'}|\mathrm{SD}\rangle = 0$, into Eqs. (28) and (29). Then we find that $\Gamma^{(2)}_{q_y}$ is of the form

$$\left(\Gamma^{(2)}_{q_y}\right)_{i_x,i'_x} = U \begin{pmatrix} -\left(T^{\mathrm{SD}}_{q_y+\pi}\right)_{i'_x,i_x} & 0 \\ 0 & \left(T^{\mathrm{SD}}_{q_y}\right)_{i_x,i'_x} \end{pmatrix} U^\dagger, \tag{57}$$

where U is an 8×8 unitary matrix whose elements are given by $U_{ij} = \delta_{2i-1,j} + \delta_{2i-8,j}$ and, in the thermodynamic limit $L_x \to \infty$, $T^{\mathrm{SD}}_{q_y}$ is a block Toeplitz matrix

$$\left(T_{q_y}\right)^{\mathrm{SD}}_{i_x,i'_x} = \int_0^{2\pi} \frac{\mathrm{d}q_x}{2\pi} e^{-2\mathrm{i}q_x(i_x-i'_x)} g^{\mathrm{SD}}_{q_y}(q_x), \tag{58}$$

with 4×4 symbol

$$g^{\mathrm{SD}}_{q_y}(q_x) = -(e^{-\mathrm{i}\sigma_z t\,\cos q_y} \otimes e^{\mathrm{i}\sigma_z \frac{q_x}{2}}) \times (I \otimes \sigma_x \cos q_x + \sigma_x \otimes \sigma_+ e^{-2\mathrm{i}t\cos q_x}) \times (e^{\mathrm{i}\sigma_z t\cos q_y} \otimes e^{-\mathrm{i}\sigma_z \frac{q_x}{2}}). \tag{59}$$

In the ballistic limit, the asymptotic form of the moments $\mathrm{Tr}\,[(\Gamma^{(2)}_{q_y})^{2m}]$ with Eq. (57) can be obtained by an analogous procedure used in Ref. [80] to derive Eq. (51). A tedious but straightforward calculation leads to the final result

$$\mathrm{Tr}\left[\left(\Gamma^{(2)}_{q_y}\right)^{2m}\right] \simeq 4\ell - 4\int_0^{2\pi} \frac{\mathrm{d}q_x}{2\pi} \times [1-(\cos q_x)^{2m}]\min(\ell, 2t|v_x(q_x)|). \tag{60}$$

Plugging it into Eq. (25) with $k = 2$, we arrive at

$$S_n \simeq L_y \int_0^{2\pi} \frac{\mathrm{d}q_x}{2\pi} h_n(\cos q_x)\min(\ell, 2t|v_x(q_x)|). \tag{61}$$

This expression is equal to Eq. (52) for the collinear dimer state. This coincidence only occurs in the limit $L_x \to \infty$, for finite L_x the entanglement entropy in these two quenches is different. We check the validity of the analytical prediction (61) in Fig. 5. It shows that, for $n \to 1$ and $n = 2$, Eq. (61) agrees well with the exact results obtained by evaluating numerically Eq. (8).

E. Diagonal dimer state

We next take as initial configuration the diagonal dimer state

$$|\mathrm{DD}\rangle = \prod_{i_x=0}^{\frac{L_x}{2}-1}\prod_{i_y=0}^{L_y-1} \frac{a^\dagger_{2i_x,i_y} - a^\dagger_{2i_x+1,i_y+1}}{\sqrt{2}}|0\rangle. \tag{62}$$

An illustration of it can be found in Fig. 2(e).

The diagonal dimer state is invariant under one-site translations in the y direction and under two-site translations in the

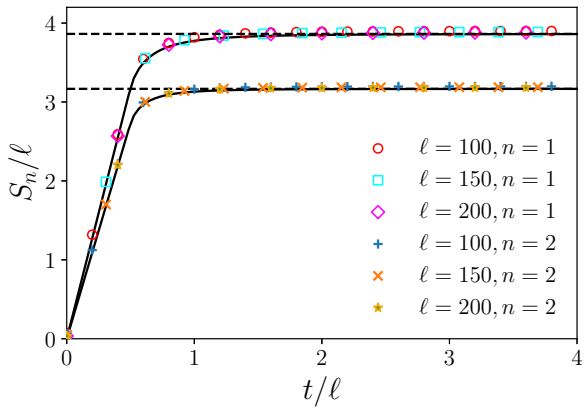

FIG. 5. Rényi entanglement entropy as a function of t/ℓ in a quench starting from the staggered dimer state for $n \to 1$ and $n = 2$ and different subsystem lengths ℓ. The solid lines correspond to the analytical prediction obtained in Eq. (61). The dashed lines indicate the saturation values (53). The symbols are the exact numerical value of the entropies calculated employing Eq. (8). We take $L_y = 10$.

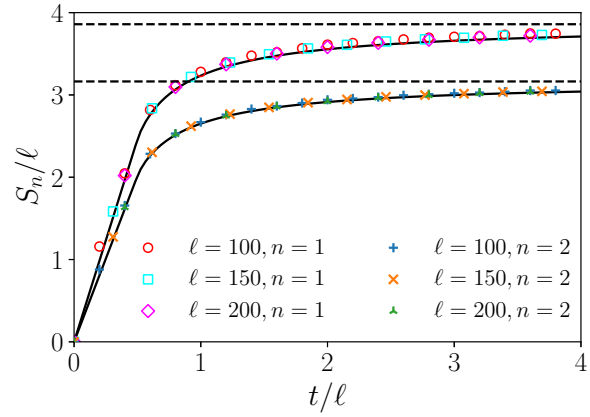

FIG. 6. Time evolution of the Rényi entanglement entropy taking as initial configuration the diagonal dimer state. We consider different Rényi indices n and subsystem sizes ℓ. The solid lines represent the analytic expression in Eq. (68). The symbols are the exact numerical entropy computed with Eq. (8). The dashed lines correspond to the saturation value predicted in Eq. (69). We set $L_y = 10$.

x direction. Therefore, we rearrange the entries of $\Gamma^{(1)}_{q_y}$ as we have done in Eq. (45). The two-point spatial correlations in the initial state are in this case

$$\langle \mathrm{DD}|a^\dagger_{\mathbf{j}} a_{\mathbf{j}'}|\mathrm{DD}\rangle = \frac{\delta_{\mathbf{j},\mathbf{j}'}}{2} - \frac{1}{4}\delta_{j_x\pm1,j'_x}\delta_{j_y\pm1,j'_y} \mp \frac{(-1)^{j_x}}{4}\delta_{j_x\pm1,j'_x}\delta_{j_y\pm1,j'_y}, \tag{63}$$

and $\langle \mathrm{DD}|a_{\mathbf{j}} a_{\mathbf{j}'}|\mathrm{DD}\rangle = 0$. Inserting them in Eqs. (28) and (29), we find that the matrix $\Gamma^{(1)}_{q_y}$ can be written as

$$\left(\Gamma^{(1)}_{q_y}\right)_{i_x,i'_x} = U \begin{pmatrix} -\left(T^{\mathrm{DD}}_{q_y}\right)_{i'_x,i_x} & 0 \\ 0 & \left(T^{\mathrm{DD}}_{-q_y}\right)_{i_x,i'_x} \end{pmatrix} U^\dagger, \tag{64}$$

where $U = I_4/2 - \sum_{\mu=x,y,z}\sigma_\mu \otimes \sigma_\mu/2$. In the thermodynamic limit $L_x \to \infty$, $T^{\mathrm{DD}}_{q_y}$ is the block Toeplitz matrix

$$\left(T^{\mathrm{DD}}_{q_y}\right)_{i_x,i'_x} = \int_0^{2\pi} \frac{\mathrm{d}q_x}{2\pi} e^{-2\mathrm{i}q_x(i_x-i'_x)} g^{\mathrm{DD}}_{q_y}(q_x), \tag{65}$$

with symbol

$$g^{\mathrm{DD}}_{\pm q_y}(q_x) = -e^{\mathrm{i}\frac{q_x}{2}\sigma_z}[\sigma_x \cos(q_x+q_y) + e^{-2\mathrm{i}t\cos q_x}\sigma_+ \sin(q_x+q_y)]e^{-\mathrm{i}\frac{q_x}{2}\sigma_z}. \tag{66}$$

The calculation of the moments $\mathrm{Tr}\,[(\Gamma^{(1)}_{q_y})^{2m}]$ with Eq. (64) in the ballistic limit is analogous to the computation of Eq. (51). We find

$$\mathrm{Tr}\left[\left(\Gamma^{(1)}_{q_y}\right)^{2m}\right] \simeq 2\ell - 2\int_0^{2\pi}\frac{\mathrm{d}q_x}{2\pi}\{1-[\cos(q_x+q_y)]^{2m}\} \times \min(\ell, 2t|v_x(q_x)|). \tag{67}$$

Substituting it into Eq. (25) with $k = 1$, we obtain that the entanglement entropy behaves as

$$S_n \simeq \sum_{q_y}\int_0^{2\pi}\frac{\mathrm{d}q_x}{2\pi} h_n[\cos(q_x+q_y)]\min(\ell, 2t|v_x(q_x)|). \tag{68}$$

Note that, unlike the previous cases, the contribution to the entropy of each mode q_y is different. At large times, $t \gg \ell/2$, the entropy saturates to

$$\lim_{t\to\infty} S_n \simeq \ell \sum_{q_y}\int_0^{2\pi}\frac{\mathrm{d}q_x}{2\pi} h_n[\cos(q_x+q_y)]. \tag{69}$$

In Fig. 6, we analyze the entanglement entropy in the quantum quench from the diagonal dimer state. We obtain an excellent agreement between the analytic result of Eq. (68) and the numerical values computed using Eq. (8).

F. Crossed dimer state

Here we consider the quantum quench starting from the crossed dimer state

$$|\mathrm{C}\rangle = \prod_{i_x=0}^{\frac{L_x}{2}-1}\prod_{i_y=0}^{\frac{L_y}{2}-1}\frac{1}{2}(a^\dagger_{2i_x,2i_y} - a^\dagger_{2i_x+1,2i_y+1}) \times (a^\dagger_{2i_x+1,2i_y} - a^\dagger_{2i_x,2i_y+1})|0\rangle, \tag{70}$$

which is schematically illustrated in Fig. 2(f). Since this configuration is invariant under two-site translations in the y direction, the entanglement entropy after the quench can be calculated by evaluating the moments $\mathrm{Tr}\,[(\Gamma^{(2)}_{q_y})^{2m}]$. To adapt the computation to the two-site translation symmetry in the x direction, we rearrange the entries of $\Gamma^{(2)}_{q_y}$ as in Eq. (55). This matrix can be calculated employing Eqs. (28) and (29) with the initial state two-point spatial correlators $\langle a^\dagger_{\mathbf{j}} a_{\mathbf{j}'}\rangle$ and $\langle a_{\mathbf{j}} a_{\mathbf{j}'}\rangle$. For the crossed dimer state, the

latter read as

$$\langle \mathrm{C}|a^\dagger_{\mathbf{j}}a_{\mathbf{j}'}|\mathrm{C}\rangle = \frac{\delta_{\mathbf{j},\mathbf{j}'}}{2} - \frac{1}{8}(\delta_{j_x+1,j'_x}\delta_{j_y+1,j'_y} + \delta_{j_x-1,j'_x}\delta_{j_y-1,j'_y} + \delta_{j_x-1,j'_x}\delta_{j_y+1,j'_y} + \delta_{j_x+1,j'_x}\delta_{j_y-1,j'_y})$$
$$- \frac{(-1)^{j_x}}{8}(\delta_{j_x+1,j'_x}\delta_{j_y+1,j'_y} - \delta_{j_x-1,j'_x}\delta_{j_y-1,j'_y} - \delta_{j_x-1,j'_x}\delta_{j_y+1,j'_y} + \delta_{j_x+1,j'_x}\delta_{j_y-1,j'_y})$$
$$- \frac{(-1)^{j_y}}{8}(\delta_{j_x+1,j'_x}\delta_{j_y+1,j'_y} - \delta_{j_x-1,j'_x}\delta_{j_y-1,j'_y} + \delta_{j_x-1,j'_x}\delta_{j_y+1,j'_y} - \delta_{j_x+1,j'_x}\delta_{j_y-1,j'_y})$$
$$- \frac{(-1)^{j_x+j_y}}{8}(\delta_{j_x+1,j'_x}\delta_{j_y+1,j'_y} + \delta_{j_x-1,j'_x}\delta_{j_y-1,j'_y} - \delta_{j_x-1,j'_x}\delta_{j_y+1,j'_y} - \delta_{j_x+1,j'_x}\delta_{j_y-1,j'_y}), \tag{71}$$

and $\langle \mathrm{C}|a_{\mathbf{i}}a_{\mathbf{i}'}|\mathrm{C}\rangle = 0$. We then obtain that $\Gamma^{(2)}_{q_y}$ is of the form

$$\left(\Gamma^{(2)}_{q_y}\right)_{i_x,i'_x} = U e^{\mathrm{i}t\sigma_z\otimes\sigma_z\otimes I\cos q_y} \times \begin{pmatrix} -\hat{m}(q_y)\otimes T^{\mathrm{C}}_{i'_x,i_x} & 0 \\ 0 & \hat{m}(q_y)\otimes T^{\mathrm{C}}_{i_x,i'_x} \end{pmatrix} \times e^{-\mathrm{i}t\sigma_z\otimes\sigma_z\otimes I\cos q_y}U^\dagger, \tag{72}$$

where $U_{ij} = \delta_{2i-1,j} + \delta_{2i-8,j}$. The matrix $\hat{m}_{q_y}$ is defined as

$$\hat{m}_{q_y} = -\sigma_z\cos q_y + \sigma_y \sin q_y, \tag{73}$$

and, in the thermodynamic limit $L_x \to \infty$, T^{C} reads as

$$T^{\mathrm{C}}_{i_x,i'_x} = \int_0^{2\pi}\frac{\mathrm{d}q_x}{2\pi}e^{-2\mathrm{i}(i_x-i'_x)}g_{\mathrm{C}}(q_x). \tag{74}$$

Here the symbol $g_{\mathrm{C}}(q_x)$ is given by

$$g_{\mathrm{C}}(q_x) = e^{\mathrm{i}\frac{q_x}{2}\sigma_z}(\sigma_x\cos q_x + \sigma_+ \sin q_x e^{-2\mathrm{i}t\,\cos q_x})e^{-\mathrm{i}\frac{q_x}{2}\sigma_z}. \tag{75}$$

Since the trace of the tensor product of two matrices is the product of the traces of the matrices, the moments $\mathrm{Tr}\,[(\Gamma^{(2)}_{q_y})^{2m}]$ in the present case are given by

$$\mathrm{Tr}\left[\left(\Gamma^{(2)}_{q_y}\right)^{2m}\right] = 2\,\mathrm{Tr}\left[\hat{m}^{2m}_{q_y}\right]\mathrm{Tr}[(T^{\mathrm{C}})^{2m}]. \tag{76}$$

By simple algebra, one finds $\mathrm{Tr}[\hat{m}^{2m}_{q_y}] = 2$ while, by employing the stationary phase method of Ref. [139], one can also obtain the asymptotic form of $\mathrm{Tr}[(T^{\mathrm{C}})^{2m}]$ in the ballistic limit

$$\mathrm{Tr}[(T^{\mathrm{C}})^{2m}] \simeq \ell - \int_0^{2\pi}\frac{\mathrm{d}q_x}{2\pi}[1-(\cos q_x)^{2m}] \times \min(\ell, 2t|v_x(q_x)|). \tag{77}$$

Therefore, putting the previous results together, the moments of the matrix (72) are

$$\mathrm{Tr}\left[\left(\Gamma^{(2)}_{q_y}\right)^{2m}\right] \simeq 4\ell - 4\int_0^{2\pi}\frac{\mathrm{d}q_x}{2\pi}[1-(\cos q_x)^{2m}] \times \min(\ell, 2t|v_x(q_x)|) \tag{78}$$

and, plugging them in Eq. (25) with $k = 2$, we finally find that

$$S_n = L_y\int_0^{2\pi}\frac{\mathrm{d}q_x}{2\pi}h_n(\cos q_x)\min(\ell, 2t|v_x(q_x)|). \tag{79}$$

In particular, the stationary value of the entanglement entropy at large times $t \gg \ell/2$ is

$$\lim_{t\to\infty} S_n \simeq V_A\int_0^{2\pi}\frac{\mathrm{d}q_x}{2\pi}h_n(\cos q_x). \tag{80}$$

In Fig. 7, we plot the entanglement entropy in the quantum quench starting from the crossed dimer state. It shows that the analytic expression obtained in Eq. (79) agrees well with the exact result obtained numerically with Eq. (8).

G. Partially filled product state

So far, we have considered initial states with a defined number of particles, i.e., eigenstates of the particle-number operator $Q = \sum_{\mathbf{i}} a^\dagger_{\mathbf{i}}a_{\mathbf{i}}$. Let us now study quenches from configurations that break this U(1) symmetry.

We can construct them using as building block the 1D product state

$$|\theta\rangle_{i_y} = \prod_{i_x=0}^{L_x-1}\left(\sin\frac{\theta}{2} + \cos\frac{\theta}{2}a^\dagger_{\mathbf{i}}\right)|0\rangle_{i_y}, \tag{81}$$

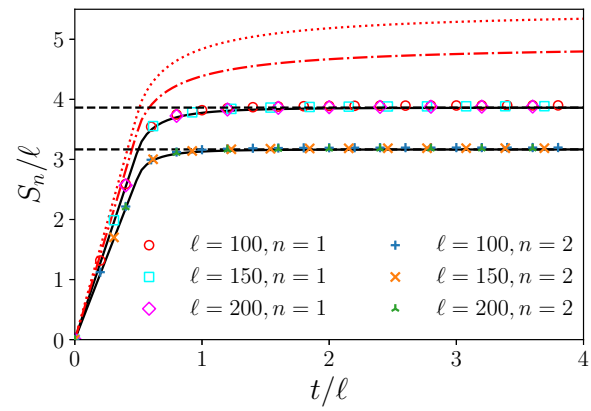

FIG. 7. Rényi entanglement entropy as a function of t/ℓ in a quench from the crossed dimer state for Rényi indices $n \to 1$ and $n = 2$ and different subsystem sizes ℓ. The solid lines represent the analytic expression obtained in Eq. (79) while the symbols are the exact value of the entropies calculated numerically using Eq. (8). The dashed lines are the saturation values at large times given by Eq. (80). The dotted and dashed-dotted lines are the predictions of the quasiparticle picture in Eq. (115) for $n \to 1$ and 2, respectively (see the discussion in the next section for the explanation of the disagreement). In all the cases, we take $L_y = 10$.

where $|0\rangle_{i_y} = \bigotimes_{i_x=0}^{L_x-1} |0\rangle_{\mathbf{i}}$ with $|0\rangle_{\mathbf{i}}$ being the local vacuum state for the **i**th site (in 1D spin language this is a tilted ferromagnetic state). The angle $\theta \in [0, \pi)$ controls the probability of finding a particle at the site **i** and, therefore, tunes how much the particle-number symmetry is broken [88]. At $\theta = 0$ (π), the state (81) is fully occupied (empty) and it preserves this U(1) symmetry, whereas it breaks it for $\theta \neq 0, \pi$; in particular, the symmetry is maximally broken at $\theta = \pi/2$.

The state (81) does not satisfy Wick theorem and, therefore, its reduced density matrix is not Gaussian and we cannot calculate the entanglement entropy from the two-point correlation matrix using Eq. (8). However, the *cat* version of (81),

$$|\mathrm{PF}\rangle_{i_y} = \frac{1}{\sqrt{2+2(\cos\theta)^{L_x}}}(|\theta\rangle_{i_y} - |-\theta\rangle_{i_y}), \tag{82}$$

does satisfy Wick theorem and its reduced density matrix is Gaussian, as explicitly shown, e.g., in Ref. [89].

From the 1D state $|\mathrm{PF}\rangle_{i_y}$, we can construct two different initial configurations in the two-dimensional square lattice, for which the entanglement entropy evolves differently after a quench to H. We study them separately in the next subsections.

1. Partially filled product state I

Let us first consider the state

$$|\mathrm{PF_I}\rangle = \bigotimes_{i_y=0}^{L_y-1} |\mathrm{PF}\rangle_{i_y}, \tag{83}$$

where $|\mathrm{PF}\rangle_{i_y}$ is defined in Eq. (81). Since (83) is invariant under one-site translations in the y direction, we can employ Eq. (25) with $k = 1$ to calculate the evolution of the entanglement entropy after the quench. The entries of the correlation matrix $\Gamma^{(1)}_{q_y}$ that enters in such equation can be determined using Eqs. (28) and (29) with the initial values of the two-point spatial correlators. In this case, given the product state structure of the initial configuration (83), we have

$$\langle \mathrm{PF_I}|a^\dagger_{\mathbf{i}} a_{\mathbf{i}'}|\mathrm{PF_I}\rangle = {}_{i_y}\langle \mathrm{PF}|a^\dagger_{i_x,i_y} a_{i'_x,i_y}|\mathrm{PF}\rangle_{i_y}\delta_{i_y,i'_y} \tag{84}$$

and

$$\langle \mathrm{PF_I}|a_{\mathbf{i}} a_{\mathbf{i}'}|\mathrm{PF_I}\rangle = {}_{i_y}\langle \mathrm{PF}|a_{i_x,i_y} a_{i'_x,i_y}|\mathrm{PF}\rangle_{i_y}\delta_{i_y,i'_y}. \tag{85}$$

The correlators for the 1D state $|\mathrm{PF}\rangle_{i_y}$ have been calculated in, e.g., Ref. [88]. Using them here, we have

$$\langle \mathrm{PF_I}|a^\dagger_{\mathbf{i}} a_{\mathbf{i}'}|\mathrm{PF_I}\rangle = \frac{\delta_{i_x,i'_x}\delta_{i_y,i'_y}}{2} - \frac{\delta_{i_y,i'_y}}{2L_x}\sum_{q_x} e^{-\mathrm{i}q_x(i_x-i'_x)}\cos\Delta_{q_x} \tag{86}$$

and

$$\langle \mathrm{PF_I}|a_{\mathbf{i}} a_{\mathbf{i}'}|\mathrm{PF_I}\rangle = -\frac{\mathrm{i}\delta_{i_y,i'_y}}{2L_x}\sum_{q_x} e^{-\mathrm{i}q_x(i_x-i'_x)}\sin\Delta_{q_x}, \tag{87}$$

with

$$\cos\Delta_{q_x} = \frac{2|\cos\theta| - \cos q_x(1+\cos^2\theta)}{1+\cos^2\theta - 2|\cos\theta|\cos q_x}, \tag{88}$$

$$\sin\Delta_{q_x} = \frac{\sin^2\theta\,\sin q_x}{1+\cos^2\theta - 2|\cos\theta|\cos q_x}. \tag{89}$$

Inserting them in Eqs. (28) and (29) and taking the limit $L_x \to \infty$, we find that $\Gamma^{(1)}_{q_y}$ is a block Toeplitz matrix

$$\left(\Gamma^{(1)}_{q_y}\right)_{i_x,i'_x} = \int_0^{2\pi} \frac{\mathrm{d}q_x}{2\pi} e^{-\mathrm{i}q_x(i_x-i'_x)} g^{\mathrm{PF}}_{q_y}(q_x), \tag{90}$$

generated by the 2×2 symbol $g^{\mathrm{PF}}_{q_y}(q_x)$:

$$g^{\mathrm{PF}}_{q_y}(q_x) = \sigma_z\cos\Delta_{q_x} + \sigma_y e^{-2\mathrm{i}t\epsilon_{\mathbf{q}}\sigma_z}\sin\Delta_{q_x}. \tag{91}$$

The moments $\mathrm{Tr}\,[(\Gamma^{(1)}_{q_y})^{2m}]$ of a block Toeplitz matrix can be calculated by applying directly the stationary phase method of Ref. [139]. In our case, we get

$$\mathrm{Tr}\left[\Gamma^{2m}_{q_y}\right] \simeq 2\ell - 2\int_0^{2\pi}\frac{\mathrm{d}q_x}{2\pi}[1-(\cos\Delta_{q_x})^{2m}] \times \min(\ell, 2t|v_x(q_x)|). \tag{92}$$

Plugging it into Eq. (25) with $k = 1$, we finally obtain that

$$S_n \simeq L_y\int_0^{2\pi}\frac{\mathrm{d}q_x}{2\pi} h_n(\cos\Delta_{q_x})\min(\ell, 2t|v_x(q_x)|). \tag{93}$$

In this case, the entropy converges at large times $t \gg \ell/2$ to the value

$$\lim_{t\to\infty} S_n \simeq V_A\int_0^{2\pi}\frac{\mathrm{d}q_x}{2\pi} h_n(\cos\Delta_{q_x}). \tag{94}$$

In Fig. 8(a), we plot the time evolution of the entanglement entropy after the quench from the state $|\mathrm{PF_I}\rangle$ for different values of the angle θ and the Rényi index n. We find that Eq. (93) agrees well with the numerical value of the entropy calculated with Eq. (8). In Fig. 8(b), we represent the stationary value of the entropy given by Eq. (94) as a function of the initial angle θ. It can be seen that the entanglement entropy monotonically increases as θ increases until $\theta = \pi/2$, the angle at which the initial state (83) maximally breaks the U(1) particle-number symmetry. This maximum value for the von Neumann entropy is $S_1^{\max} = V_A[2\,\log(2) - 1]$.

2. Partially filled product state II

From the 1D state (81), we can also construct the configuration

$$|\mathrm{PF_{II}}\rangle = \bigotimes_{i_x=0}^{L_x-1} |\mathrm{PF}\rangle_{i_x}. \tag{95}$$

The difference compared to state (83) is that this is a product state in the x direction while the other was in the y direction. Since the native 1D state (82) is a cat and not a product state, the two definitions are inequivalent. This state $|\mathrm{PF_{II}}\rangle$ is invariant under one-site translations in the y and x directions. Since it is a product state along the x direction its two-point spatial correlation functions satisfy

$$\langle \mathrm{PF_{II}}|a^\dagger_{\mathbf{i}} a_{\mathbf{i}'}|\mathrm{PF_{II}}\rangle = {}_{i_x}\langle \mathrm{PF}|a^\dagger_{i_x,i'_y} a_{i_x,i'_y}|\mathrm{PF}\rangle_{i_x}\delta_{i_x,i'_x} \tag{96}$$

and

$$\langle \mathrm{PF_{II}}|a_{\mathbf{i}} a_{\mathbf{i}'}|\mathrm{PF_{II}}\rangle = {}_{i_x}\langle \mathrm{PF}|a_{i_x,i_y} a_{i_x,i'_y}|\mathrm{PF}\rangle_{i_x}\delta_{i_y,i'_x}. \tag{97}$$

As we did in the other partially filled product state, we can apply the results of Ref. [88] for the correlations of the 1D

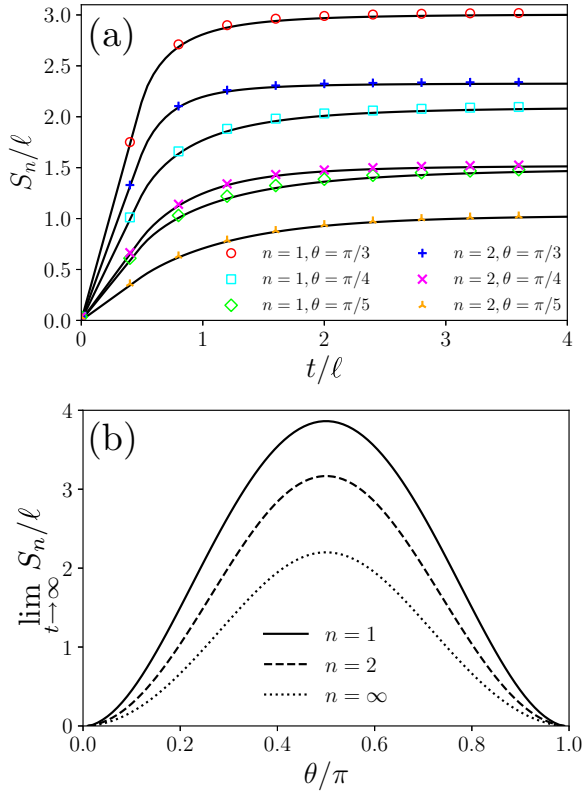

FIG. 8. (a) Time evolution of the Rényi entanglement entropy after a quench from the state $|\mathrm{PF_I}\rangle$, considering different angles θ for the initial configuration and Rényi indices n. The solid lines correspond to the analytic prediction found in Eq. (93). The symbols are the exact values computed numerically with Eq. (8). (b) Saturation value at large times of the Rényi entanglement entropy given in Eq. (94) as a function of the initial angle θ for different Rényi indices n. In all cases, we set $\ell = 200$ and $L_y = 10$.

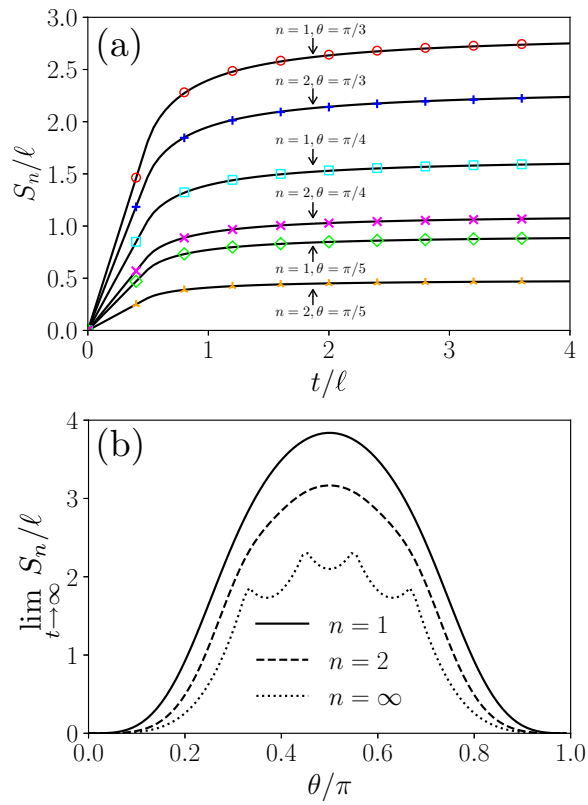

FIG. 9. (a) Rényi entanglement entropy as a function of t/ℓ after a quench from the state $|\mathrm{PF_{II}}\rangle$. We take several angles θ in the initial state and Rényi indices $n \to 1$ and $n = 2$. The solid lines are the analytic expression derived in Eq. (102) while the symbols represent the exact result obtained numerically employing Eq. (8). (b) We represent the saturation value at large times of Rényi entanglement entropy predicted in Eq. (103) versus the initial angle θ. In all cases, we fix $\ell = 200$ and $L_y = 10$.

state $|\mathrm{PF}\rangle_{i_x}$. Then we have

$$\langle \mathrm{PF_{II}}|a_{\mathbf{i}}^{\dagger}a_{\mathbf{i}'}|\mathrm{PF_{II}}\rangle = \frac{\delta_{i_x,i_x'}\delta_{i_y,i_y'}}{2} - \frac{\delta_{i_x,i_x'}}{2L_y}\sum_{q_y} e^{-\mathrm{i}q_y(i_y-i_y')}\cos\Delta_{q_y} \tag{98}$$

and

$$\langle \mathrm{PF_{II}}|a_{\mathbf{i}}a_{\mathbf{i}'}|\mathrm{PF_{II}}\rangle = -\frac{\mathrm{i}\delta_{i_x,i_x'}}{2L_y}\sum_{q_y} e^{-\mathrm{i}q_y(i_y-i_y')}\sin\Delta_{q_y}. \tag{99}$$

Inserting these correlators in Eqs. (28) and (29) and taking the thermodynamic limit $L_x \to \infty$, the matrix $\Gamma^{(1)}_{q_y}$ that gives the entanglement entropy (25) is block Toeplitz,

$$\left(\Gamma^{(1)}_{q_y}\right)_{i_x,i_x'} = \int_0^{2\pi}\frac{\mathrm{d}q_x}{2\pi}e^{-\mathrm{i}q_x(i_x-i_x')}g^{\mathrm{PF}}_{q_x}(q_y), \tag{100}$$

in which the symbol is the same as in Eq. (91) but exchanging the moments q_x and q_y.

As in the previous examples, in the ballistic limit, the asymptotic form of the moments $\mathrm{Tr}\,[(\Gamma^{(1)}_{q_y})^{2m}]$ for Eq. (100) can be obtained by applying the stationary phase method for block Toeplitz matrices of Ref. [139]. Here we find

$$\mathrm{Tr}\big[\big(\Gamma^{(1)}_{q_y}\big)^{2m}\big] \simeq 2\ell - 2[1-(\cos\Delta_{q_y})^{2m}] \times \int_0^{2\pi}\frac{\mathrm{d}q_x}{2\pi}\min\left(\ell, 2t|v_x(q_x)|\right). \tag{101}$$

Applying this result in Eq. (25) with $k = 1$, we get that the entanglement entropy evolves in time after the quench as

$$S_n \simeq \sum_{q_y} h_n(\cos\Delta_{q_y})\int_0^{2\pi}\frac{\mathrm{d}q_x}{2\pi}\min\left(\ell, 2t|v_x(q_x)|\right), \tag{102}$$

and saturates to

$$\lim_{t\to\infty} S_n = \ell\sum_{q_y} h_n(\cos\Delta_{q_y}) \tag{103}$$

at large times $t \gg \ell/2$.

Figure 9(a) shows the entanglement entropy of the time-evolved state $|\mathrm{PF_{II}}(t)\rangle$, comparing the analytic result of Eq. (102) (solid lines) with the exact value (symbols) obtained numerically with Eq. (8) for several initial angles θ and Rényi index n. In Fig. 9(b), we plot the saturation value of the entanglement entropy found in Eq. (103) as a function of θ. We can see that, as in the case of the state $|\mathrm{PF_I}\rangle$, the saturation

value is maximum at $\theta = \pi/2$ (at least for $n = 1, 2$), at which the particle-number symmetry is maximally broken at $t = 0$, although it is not in general monotonic in θ. Figure 9(b) also shows that, for $n = \infty$, the Rényi entanglement entropy presents a nonanalytic behavior as a function of θ. In this limit, the Rényi entanglement entropy is given by the largest eigenvalue $\lambda_{\max}$ of the reduced density matrix ρ_A such that $S_\infty = -\log \lambda_{\max}$. Therefore, the nonanalytic points indicate that there is a level crossing between the two largest eigenvalues of the reduced density matrix at those values of θ. These nonanalyticities disappear when L_y is sufficiently large.

V. QUASIPARTICLE PICTURE

In this section, we discuss the physical interpretation of the results of the previous section in terms of the *quasiparticle picture*, originally developed for one-dimensional integrable systems [29,31].

The idea of the quasiparticle picture is the following: in one dimension the quench generates uniformly pairs of entangled quasiparticles that propagate ballistically in opposite directions with opposite momenta. Therefore, the entanglement at time t after the quench is proportional to the number of pairs of entangled quasiparticles that are shared by subsystem A and its complement B:

$$S_n = \int_0^{2\pi} \frac{\mathrm{d}q}{2\pi} s_n(q) \min\left(\ell, 2|v(q)|t\right), \tag{104}$$

where $v(q)$ is the velocity of the quasiparticle with momentum q and $s_n(q)$ its contribution to the entanglement. The function $\min\left(\ell, 2|v(q)|t\right)$ counts the quasiparticles that are shared by subsystem A and its complement at time t.

However, in $d > 1$ as in this paper, the multiplet structure of the quasiparticles is generically much more complicated than simple pairs and their counting is far from trivial. Fortunately, the dimensional reduction comes in our help, leading to extremely simple results. Indeed, since the Rényi entanglement entropy can be decomposed in the single-interval entanglement entropies of decoupled 1D chains, we can directly apply the quasiparticle picture in each decoupled chain, which are labeled by the transverse momentum $q_y = 2\pi n_y/L_y$. Therefore, after the quench, in the n_y-chain pairs of entangled excitations propagate with momentum $\pm q_x$ and velocity $v_x(q_x) = \partial_{q_x}\epsilon_{\mathbf{q}}$. If we denote the contribution to the entanglement entropy of each pair of entangled modes as $s_n(\mathbf{q})$ and sum over all the decoupled chains the result (104), then we expect

$$S_n = \sum_{n_y=0}^{\frac{L_y}{k}-1} \int_0^{2\pi} \frac{\mathrm{d}q_x}{2\pi} s_n(\mathbf{q}) \min\left(\ell, 2|v_x(q_x)|t\right). \tag{105}$$

Equation (105) predicts that the entanglement entropy increases linearly for $t < \ell/2$ and tends to a constant at large times $t \gg \ell/2$; this is the qualitative behavior that we have found in all the examples studied in Sec. IV.

To obtain quantitative predictions from Eq. (105), we have to determine a specific expression of $s_n(\mathbf{q})$. For one-dimensional free fermion systems, as proposed in Ref. [31] for generic integrable systems, the analogous function $s_n(q)$ can be read off from the limit $t \to \infty$, in which the reduced density matrix $\rho_A(t)$ is expected to relax to a GGE. We can apply the same idea here. In particular, for the 2D free fermion model (1), one may expect that the infinite-time limit of $\rho_A(t)$ exists and it is described by a GGE, i.e.,

$$\lim_{t\to\infty} \rho_A(t) = \mathrm{Tr}_B(\rho^{\mathrm{GGE}}) \equiv \rho_A^{\mathrm{GGE}}. \tag{106}$$

As in one dimension [140], since the postquench Hamiltonian is diagonal in terms of the modes $\tilde{a}_{\mathbf{q}}^\dagger$ and $\tilde{a}_{\mathbf{q}}$, the GGE can be written in terms of the the conserved mode occupation numbers $\hat{n}_{\mathbf{q}} = \tilde{a}_{\mathbf{q}}^\dagger \tilde{a}_{\mathbf{q}}$ as

$$\rho^{\mathrm{GGE}} = \frac{e^{-\sum_{\mathbf{q}} \lambda_{\mathbf{q}} \hat{n}_{\mathbf{q}}}}{\mathrm{Tr}(e^{-\sum_{\mathbf{q}} \lambda_{\mathbf{q}} \hat{n}_{\mathbf{q}}})}, \tag{107}$$

where the Lagrange multipliers $\lambda_{\mathbf{q}}$ are determined by the expectation value of $\hat{n}_{\mathbf{q}}$,

$$\mathrm{Tr}(\hat{n}_{\mathbf{q}} \rho^{\mathrm{GGE}}) = \langle \psi_0 | \hat{n}_{\mathbf{q}} | \psi_0 \rangle \equiv n_{\mathbf{q}}. \tag{108}$$

We stress that this is valid under the quite general assumption that non-Abelian charges like $\sum_j (-1)^j c_j c_{j+m}$ are not activated by the initial state; their activation would lead to an altered dynamics [89,141].

If the reduced density matrix $\rho_A(t)$ relaxes to the GGE as in Eq. (106), then the Rényi entanglement entropy for $\rho_A(t)$ at large times must be equal to the entropy of the statistical ensemble ρ_A^{GGE},

$$\lim_{t\to\infty} S_n(\rho_A(t)) = S_n\left(\rho_A^{\mathrm{GGE}}\right). \tag{109}$$

We can deduce the specific form of $s_n(\mathbf{q})$ from the above equation as follows. For a large subsystem with volume V_A, $S_n(\rho_A^{\mathrm{GGE}})$ is proportional to V_A because it is an extensive thermodynamic quantity. Hence, the entropy $S_n(\rho_A^{\mathrm{GGE}})$ is given by the volume of subsystem A times the density of the Rényi entropy evaluated in the GGE of Eq. (107). That is,

$$\begin{aligned} S_n\left(\rho_A^{\mathrm{GGE}}\right) &= \frac{V_A}{L_x L_y} S_n\left(\rho^{\mathrm{GGE}}\right) \\ &= \ell \sum_{n_y=0}^{L_y-1} \int_0^{2\pi} \frac{\mathrm{d}q_x}{2\pi} h_n(2n_{\mathbf{q}} - 1), \end{aligned} \tag{110}$$

where the function $h_n(x)$ is defined in Eq. (9). In the second line, we have taken the thermodynamic limit $L_x \to \infty$ to derive it. On the other hand, if we take the large-time limit $t \to \infty$ in Eq. (105), we obtain

$$\lim_{t\to\infty} S_n(\rho_A) = \ell \sum_{n_y=0}^{L_y/k-1} \int_0^{2\pi} \frac{\mathrm{d}q_x}{2\pi} s_n(\mathbf{q}). \tag{111}$$

Comparing Eqs. (110) and (111) and naturally grouping together the chains with equal n_y modulo k, we can conclude that

$$s_n(\mathbf{q}) = \sum_{j=0}^{k-1} h_n(2n_{q_x, q_y + \frac{2\pi j}{k}} - 1). \tag{112}$$

Finally, plugging this result into Eq. (105), we find

$$S_n = \sum_{n_y=0}^{L_y-1} \int_0^{2\pi} \frac{\mathrm{d}q_x}{2\pi} h_n(2n_{\mathbf{q}} - 1) \min\left(\ell, 2t|v_x(q_x)|\right). \tag{113}$$

We emphasize that this prediction assumes the thermodynamic limit in the x direction, but the value of L_y is an arbitrary integer, also as small as 1 or 2.

The quasiparticle formula (113) coincides with the analytic expressions found for most of the particular initial states investigated in Sec. IV. For example, the mode occupation number for the collinear Mott insulator state (30) is $n_{\mathbf{q}} = \frac{1}{2}$ and, substituting it in Eq. (113), we find Eq. (37). Also, the occupation number for the Mott insulator state (39) is $n_{\mathbf{q}} = \frac{1}{2}$. In a similar way, it is straightforward to check that the prediction of the quasiparticle picture (113) reproduces the analytic expressions for the entanglement entropy obtained in Eqs. (52) (collinear and staggered dimer states), (68) (diagonal dimer state), (93) (partially filled product state I), and (102) (partially filled product state II).

The coincidence at large times between the Rényi entanglement entropies of $\rho_A(t)$ and of the corresponding GGE is not a sufficient condition to prove that $\rho_A(t)$ relaxes to the latter. However, the results presented in this paper straightforwardly demonstrate that, for all the initial states for which the quasiparticle picture (113) works, the spatial two-point correlation functions converge to the corresponding GGE value in the large-time limit. Since $\rho_A(t)$ is Gaussian, it is univocally determined by the two-point correlation matrix in A. Therefore, the GGE's ability to capture the large-time behavior of the spatial two-point correlators implies (i) that it fully describes the stationary state of the subsystem and (ii) the validity of Eq. (106).

However, the situation is different for the crossed dimer state discussed in Sec. IV F. In this case, the mode occupation number is

$$n_{\mathbf{q}} = \langle \mathrm{C}|\hat{n}_{\mathbf{q}}|\mathrm{C}\rangle = \frac{1-\cos q_x \cos q_y}{2} \tag{114}$$

and, if we plug it in the quasiparticle prediction (113), then we obtain

$$S_n = \sum_{n_y=0}^{L_y-1} \int_0^{2\pi} \frac{\mathrm{d}q_x}{2\pi} h_n(\cos q_x \cos q_y) \min\left(\ell, 2t|v_x(q_x)|\right), \tag{115}$$

which does not match the correct result in Eq. (79), as also shown in Fig. 7.

Comparing Eqs. (79) and (115), it is clear that the reason why the quasiparticle picture breaks down is that the identification (112) does not hold. Since this identity has been derived assuming Eq. (109), the mismatch means that, in this particular quench, the reduced density matrix $\rho_A(t)$ does not tend to ρ_A^{GGE} at $t \to \infty$. In the following section, we will discern the reason why this occurs.

VI. EXISTENCE OF STATIONARY STATE

In the previous section, we have found that the prediction of the quasiparticle picture (113) does not match the correct result (79) for the crossed dimer state. We claimed that the reason for this disagreement is that the reduced density matrix $\rho_A(t)$ does not relax to the GGE ρ_A^{GGE} at large times. In this section, we show that, in two-dimensional free fermionic systems, the reduced density matrix $\rho_A(t)$ does not tend to a stationary state after quenches from certain particular initial configurations, including the crossed dimer state. Furthermore, we derive a criterion which allows us to know whether the stationary state exists or not for a given initial state and how the quasiparticle picture must be modified in its absence.

A. Absence of stationary state

To show that $\rho_A(t)$ does not relax to a stationary state for particular initial states, we start by decomposing the postquench Hamiltonian (1) as

$$H = H^X + H^Y, \tag{116}$$

where

$$H^X = \sum_{i_y=0}^{L_y-1} H^X_{i_y} = -\frac{1}{2}\sum_{i_y=0}^{L_y-1}\sum_{i_x=0}^{L_x-1} a^\dagger_{i_x+1,i_y} a_{i_x,i_y} + \mathrm{H.c.}, \tag{117}$$

and

$$H^Y = \sum_{i_x=0}^{L_x-1} H^Y_{i_x} = -\frac{1}{2}\sum_{i_x=0}^{L_x-1}\sum_{i_y=0}^{L_y-1} a^\dagger_{i_x,i_y+1} a_{i_x,i_y} + \mathrm{H.c.}. \tag{118}$$

As clear from the above equations, the terms H^X and H^Y only contain fermion hoppings in the x and y direction, respectively.

Observe that, in terms of the Fourier modes (2), H^X and H^Y are diagonal,

$$H^X = -\sum_{\mathbf{q}} \cos q_x \tilde{a}^\dagger_{\mathbf{q}} \tilde{a}_{\mathbf{q}}, \tag{119}$$

$$H^Y = -\sum_{\mathbf{q}} \cos q_y \tilde{a}^\dagger_{\mathbf{q}} \tilde{a}_{\mathbf{q}}, \tag{120}$$

and, therefore, they commute with each other. This allows us to write the time-evolved state $|\psi(t)\rangle$ as

$$|\psi(t)\rangle = e^{-\mathrm{i}tH^Y}|\psi_X(t)\rangle, \tag{121}$$

where $|\psi_X(t)\rangle = e^{-\mathrm{i}tH^X}|\psi_0\rangle$ is the time-evolved state after a quantum quench with a Hamiltonian in which the fermion hopping is allowed only in the x direction (i.e., L_y copies of 1D chains). Accordingly, the reduced density matrix $\rho_A(t)$ can be written as

$$\rho_A(t) = \mathrm{Tr}_B(e^{-\mathrm{i}tH^Y}|\psi_X(t)\rangle\langle\psi_X(t)|e^{\mathrm{i}tH^Y}). \tag{122}$$

Given its definition in Eq. (118), we have $[H^Y_{i_x}, H^Y_{i'_x}] = 0$; then the time-evolution operator $e^{-\mathrm{i}tH^Y}$ in Eq. (122) can be decomposed into two operators that, respectively, act only on the subsystems A and B as

$$e^{-\mathrm{i}tH^Y} = U_A(t)U_B(t) \tag{123}$$

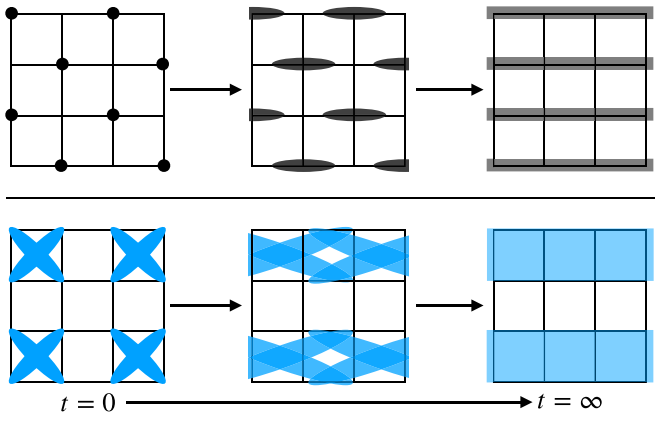

FIG. 10. Schematic representation of time evolution of the reduced density matrix $\rho_{X,A}(t)$, introduced in Eq. (126), after quenches from the Mott insulator state (upper panel) and the crossed dimer state (lower panel).

with

$$U_A(t) = \prod_{i_x=0}^{\ell-1} e^{-itH^Y_{i_x}}, \; U_B(t) = \prod_{i_x=\ell}^{L_x-1} e^{-itH^Y_{i_x}}. \tag{124}$$

Note that U_A acts only on subsystem A and hence it can be taken out the partial trace Tr_B. Therefore, we can rewrite Eq. (122) as

$$\rho_A(t) = U_A(t)\rho_{X,A}(t)U_A^\dagger(t), \tag{125}$$

where

$$\rho_{X,A}(t) = \mathrm{Tr}_B|\psi_X(t)\rangle\langle\psi_X(t)|. \tag{126}$$

Note that, in the latter expression, U_B and $U_B^\dagger$ cancel each other in the partial trace Tr_B due to the cyclic property. From Eq. (125), we conclude that, when $[U_A(t), \rho_{X,A}(\infty)] \neq 0$, the limit $\lim_{t\to\infty}\rho_A(t)$ does not exist, i.e., there is no stationary state.

B. Condition for the existence of stationary state

Having established that the existence of a stationary state is related to the vanishing of the commutator $[U_A, \rho_{X,A}(\infty)]$, the next natural step is to determine under which conditions this commutator is not zero. In Appendix A, we prove the following. If we assume that $\rho_{X,A}(t)$ relaxes to a stationary state, i.e., $\lim_{t\to\infty}\rho_{X,A}(t)$ exists, then the stationary state of $\rho_A(t)$ exists if and only if $\rho_{X,A}(t)$ restores the translational symmetry in the y direction for large times, that is

$$\mathcal{T}_A(\lim_{t\to\infty}\rho_{X,A}(t))\mathcal{T}_A^{-1} = \lim_{t\to\infty}\rho_{X,A}(t), \tag{127}$$

where $\mathcal{T}_A$ is the translation operator in the y-direction action on subsystem A.

This result allows us to know whether the stationary state exists or not from $\rho_{X,A}$. For example, in Fig. 10, we schematically represent the time evolution of $\rho_{X,A}(t)$ in quenches starting from the Mott insulator and the crossed dimer states. In the case of the Mott insulator state, after a long time, the hopping in the x direction makes the distribution of fermions uniform for every i_yth row, and the translational symmetry in the y direction is restored. Hence, the stationary state exists according to the result announced before. On the other hand, for the crossed dimer state, since the hopping in the x direction does not change the amount of entanglement between each row, after long times, the entanglement between $2i_y$th and $(2i_y+1)$th rows in the initial state remains, while no entanglement appears between $(2i_y-1)$th and $2i_y$th rows. This means that $\rho_{X,A}$ for the crossed dimer state never restores the translational symmetry in the y direction. Therefore, the reduced density matrix $\rho_A(t)$ does not relax to a stationary state in this case.

In general, as we show in Appendix B, the density matrix $\rho_{X,A}(t)$ restores the translational invariance in the y direction at large times, i.e., Eq. (127) is satisfied, if and only if

$$\langle\psi_0|\tilde{a}^\dagger_{q_x,q_y}\tilde{a}_{q_x,q_y'}|\psi_0\rangle = 0 \;\forall\; q_x, q_y \neq q_y'. \tag{128}$$

Therefore, we can conclude that $\rho_A(t)$ relaxes to a stationary state at large times if and only if the initial state satisfies Eq. (128). In fact, one can check that such correlator is always zero for all the initial states discussed in Sec. IV except for the crossed dimer state, for which we have

$$\langle \mathrm{C}|\tilde{a}^\dagger_{q_x,q_y}\tilde{a}_{q_x,q_y+\pi}|\mathrm{C}\rangle = -\frac{\mathrm{i}}{2}\cos q_x \sin q_y. \tag{129}$$

C. Entanglement entropy in the absence of stationary state: The crossed dimer state

Although, as we have just seen, there is not a stationary state in a quench from the crossed dimer state, in Sec. IV we showed that the entanglement entropy saturates to a constant value at large times. This behavior can be explained as follows. According to Eq. (125), the reduced density matrices $\rho_A(t)$ and $\rho_{X,A}(t)$ are related by a unitary transformation. This means that their entropies are equal,

$$S_n(\rho_A(t)) = S_n(\rho_{X,A}(t)). \tag{130}$$

Therefore, this identity implies that, if $\rho_{XA}(t)$ relaxes to a stationary state, then the entropy tends to a constant value at large times, even if the limit $\lim_{t\to\infty}\rho_A(t)$ does not exist.

The missing point is to determine the stationary value of the entropy in the absence of stationary state for $\rho_A(t)$. We have shown that, if $[U_A, \rho_{X,A}(\infty)] = 0$, then both $\rho_A(t)$ and $\rho_{X,A}(t)$ relax to the same stationary state, which is described by a GGE that can be built either from the local conserved charges of $H = H^X + H^Y$ or of H^X. However, the set of conserved charges of H^X is not equal to that of the total Hamiltonian H. Therefore, if $\rho_A(t)$ tends to a stationary state, only the charges shared by H^X and H can be activated. On the contrary, if there is not stationary state for $\rho_A(t)$, it exists the possibility that charges only conserved by H^X can be activated. In such cases, the entanglement entropies derived from the GGEs associated to H and H^X are different, and the correct stationary value of the entanglement entropy is given by the latter. This explains why the quasiparticle picture discussed in Sec. V does not work for the crossed dimer state, for which $\rho_A(t)$ does not relax as we have already shown.

In fact, for this initial state, we find that, to obtain the saturation value of Eq. (80) at large times, the correct GGE

should be built with the following conserved charges:

$$\hat{n}^{\pm}_{q_x,i_y} \equiv \frac{1}{\sqrt{2}}(d^{\dagger}_{q_x,2i_y} \pm d^{\dagger}_{q_x,2i_y+1})(d_{q_x,2i_y} \pm d_{q_x,2i_y+1}), \quad (131)$$

where $q_x = 0, \ldots, 2\pi(L_x-1)/L_x$, $i_y = 0, \ldots, L_y/2-1$, and $\hat{d}_{q_x,i_y}$ is the partial Fourier transform of the fermionic $a_{\mathbf{i}}$ with respect to the x direction

$$d_{q_x,i_y} \equiv \frac{1}{\sqrt{L_x}} \sum_{i_x=0}^{L_x-1} e^{-\mathrm{i}q_x i_x} a_{\mathbf{i}}. \quad (132)$$

By simple algebra, one finds that $\{\hat{n}^{\pm}_{q_x,i_y}\}$ commute with H^X while they do not commute with the total Hamiltonian $H = H^X + H^Y$.

In the same way as in Eq. (110), we can calculate the entropy of a GGE built with the charges $\{n^{\pm}_{q_x,y_i}\}$. In the thermodynamic limit $L_x \to \infty$, it is

$$S_n = \ell \sum_{i_y=0}^{\frac{L_y}{2}-1} \int_0^{2\pi} \frac{\mathrm{d}q_x}{2\pi} [h_n(2n^{+}_{q_x,i_y}-1) + h_n(2n^{-}_{q_x,i_y}-1)], \quad (133)$$

where we have introduced $n^{\pm}_{q_x,i_y} = \langle\psi_0|\hat{n}^{\pm}_{q_x,i_y}|\psi_0\rangle$. In particular, for the crossed dimer state, we obtain

$$n^{\pm}_{q_x,i_y} = \langle \mathrm{C}|\hat{n}^{\pm}_{q_x,i_y}|\mathrm{C}\rangle = \frac{1 \pm \cos q_x}{2}. \quad (134)$$

Plugging it into Eq. (133), we indeed recover the large-time limit of the evolution from the crossed dimer state in Eq. (80). At this point, Eq. (79) for the finite-time evolution is recovered by a straightforward application of the quasiparticle picture.

In Appendix C, we consider a quench from another initial configuration in which $\rho_A(t)$ does not relax to a stationary state and show that, also in this case, the large-time behavior of the entanglement entropy is captured by a GGE built with from the charges of H^X instead of H.

VII. CONCLUSIONS

To summarize, we studied the time evolution of the entanglement entropy following quantum quenches in a translationally invariant 2D free fermion lattice. We have considered different initial Gaussian configurations that present a periodic pattern in both directions of the system. By applying dimensional reduction and exploiting the well-known results for 1D free fermionic chains, we analytically determined the exact behavior of the Rényi entanglement entropies after the quench. We found that, for most of the initial states, the standard quasiparticle picture developed for 1D systems can be readily adapted to correctly explain the evolution of the entropy. Instead, for one particular initial state, the quasiparticle picture does not generalize straightforwardly because the Rényi entanglement entropies saturate to a value different from the one predicted by the GGE built with the local conserved charges of the postquench Hamiltonian. We traced back the origin of this disagreement to the absence of a stationary limit for the reduced density matrix. Starting from this observation, we deduced that the correct stationary entanglement entropy for this initial state is given by the GGE constructed with the local conserved charges of a Hamiltonian with only hoppings in the longitudinal direction. We also obtained the general conditions for the existence of the stationary limit of the reduced density matrix, which are related to the restoration of the translational symmetry in the transverse direction at large times.

The dimensional reduction approach employed here can be easily generalized to study the time evolution in two-dimensional free fermionic systems of other quantities for which there are exact results in one dimension. These include the entanglement negativity [71–74], charge fluctuations [82,142], symmetry-resolved entanglement entropies [79–83], and the recently introduced entanglement asymmetry [88–90,143]. The latter measures how much a symmetry is broken in a subsystem, and has been employed to observe a quantum version [88] of the Mpemba effect [144–147]. A relevant question is whether this effect may also occur in higher dimensions and under what conditions it happens. Another easy but interesting generalization would be to use dimensional reduction to study quench problems in 2D free-bosonic models to contrast with existing field theory literature [134].

Note added. Recently, we became aware of the parallel work [148], where also the entanglement entropy of 2D free fermion systems is studied. However, in this paper the dimensional reduction is not used and the emphasis is more on the shape on the entangling region rather than on the different initial states.

ACKNOWLEDGMENTS

We thank V. Alba, S. Murciano, and C. Rylands for fruitful discussions. S.Y. is supported by Grant-in-Aid for JSPS Fellows (Grant No. JP22KJ2775). P.C. and F.A. acknowledge support from European Research Council (ERC) under Consolidator Grant No. 771536 [New states of Entangled Matter Out of equilibrium (NEMO)]. We thank the authors of Ref. [148] for sharing their results with us before submission.

APPENDIX A: PROOF OF THE CONDITION OF EQ. (127) FOR THE EXISTENCE OF STATIONARY STATE

In this Appendix, we prove that reduced density matrix $\rho_A(t)$ relaxes to a stationary state if and only if Eq. (127) holds. In other words, the goal of the Appendix is to prove that the following two propositions are necessary and sufficient conditions for each other:

Proposition 1. The limit

$$\lim_{t\to\infty} \rho_A(t)$$

exists.

Proposition 2. For large times, $\rho_{X,A}(t)$ in Eq. (126) restores the translational symmetry in the y direction, i.e., the following equation holds:

$$\mathcal{T}_A \rho_{X,A}(\infty) \mathcal{T}_A^{-1} = \rho_{X,A}(\infty).$$

To this end, we make the following assumptions:

Assumption 1. $\rho_{X,A}(t)$ relaxes to the GGE associated to H^X [cf. Eq. (117)] at large time, i.e.,

$$\lim_{t\to\infty} \rho_{X,A}(t) = \rho_{X,A}^{\mathrm{GGE}}. \tag{A1}$$

Assumption 2. If the stationary state for $\rho_A(t)$ exists, then

$$\lim_{t\to\infty} \rho_A(t) = \rho_A^{\mathrm{GGE}}, \tag{A2}$$

where ρ_A^{GGE} is the GGE built from the conserved charges of H.

Note that we can use Assumption 2 only when Proposition 1 is true.

To prove Proposition 1 $\Longleftrightarrow$ Proposition 2, we first show that Proposition 1 is true if and only if the following proposition is true:

Proposition 3. $\rho_{X,A}(t)$ converges to ρ_A^{GGE} for large times, i.e.,

$$\rho_{X,A}^{\mathrm{GGE}} = \rho_A^{\mathrm{GGE}}.$$

Proposition 3 $\Longrightarrow$ Proposition 1 can be shown as follows: from Eq. (125),

$$\lim_{t\to\infty} \rho_A(t) = \lim_{t\to\infty} U_A(t)\rho_{A,X}(t)U_A^\dagger(t). \tag{A3}$$

Assumption 1 and Proposition 3 allow us to replace $\rho_{A,X}$ in the above equation with ρ_A^{GGE}, which reads as

$$\lim_{t\to\infty} \rho_A(t) = \lim_{t\to\infty} U_A(t)\rho_A^{\mathrm{GGE}}U_A(t)^\dagger = \rho_A^{\mathrm{GGE}}. \tag{A4}$$

Here we have used $[U_A(t), \rho_A^{\mathrm{GGE}}] = 0$ in the last equality. The above equation clearly shows that

$$\text{Proposition 3} \Longrightarrow \text{Proposition 1}. \tag{A5}$$

Proposition 1 $\Longrightarrow$ Proposition 3 can also be shown in a similar way: from Eq. (125),

$$\lim_{t\to\infty} \rho_{X,A}(t) = \lim_{t\to\infty} U_A^\dagger(t)\rho_A(t)U_A(t). \tag{A6}$$

Proposition 1 and Assumption 2 allow us to replace ρ_A in the above equation with ρ_A^{GGE}, which results in

$$\lim_{t\to\infty} \rho_{X,A}(t) = \lim_{t\to\infty} U_A^\dagger(t)\rho_A^{\mathrm{GGE}}U_A(t) = \rho_A^{\mathrm{GGE}}. \tag{A7}$$

Here we again used $[U_A(t), \rho_A^{\mathrm{GGE}}] = 0$ in the last equality. From the previous equation, we can conclude that

$$\text{Proposition 1} \Longrightarrow \text{Proposition 3}. \tag{A8}$$

Equations (A5) and (A8) imply

$$\text{Proposition 1} \Longleftrightarrow \text{Proposition 3}. \tag{A9}$$

By (A9), proving Proposition 1 $\Longleftrightarrow$ Proposition 2 is equivalent to show Proposition 2 $\Longleftrightarrow$ Proposition 3. Let us therefore prove the latter.

Proposition 3 $\Longrightarrow$ Proposition 2 can be shown as follows: from Proposition 3, we obtain

$$\mathcal{T}_A\rho_{X,A}^{\mathrm{GGE}}\mathcal{T}_A^{-1} = \mathcal{T}_A\rho_A^{\mathrm{GGE}}\mathcal{T}_A^{-1} \tag{A10}$$

$$= \mathrm{Tr}_B\left[\mathcal{T}_A\rho^{\mathrm{GGE}}\mathcal{T}_A^{-1}\right]. \tag{A11}$$

Inserting the identity $\mathcal{T}_B^{-1}\mathcal{T}_B$ in Tr_B in the above equation and using the cyclic property of trace, we obtain

$$\mathcal{T}_A\rho_{X,A}^{\mathrm{GGE}}\mathcal{T}_A^{-1} = \mathrm{Tr}_B\left[\mathcal{T}_B\mathcal{T}_A\rho^{\mathrm{GGE}}\mathcal{T}_A^{-1}\mathcal{T}_B^{-1}\right]. \tag{A12}$$

According to Eq. (107), ρ^{GGE} is invariant under translations in the y direction, namely,

$$\mathcal{T}_B\mathcal{T}_A\rho^{\mathrm{GGE}}\mathcal{T}_A^{-1}\mathcal{T}_B^{-1} = \rho^{\mathrm{GGE}}. \tag{A13}$$

Substituting it into Eq. (A12), we obtain

$$\mathcal{T}_A\rho_{X,A}^{\mathrm{GGE}}\mathcal{T}_A^{-1} = \rho_A^{\mathrm{GGE}} \tag{A14}$$

and using Proposition 3

$$\mathcal{T}_A\rho_{X,A}^{\mathrm{GGE}}\mathcal{T}_A^{-1} = \rho_{X,A}^{\mathrm{GGE}}. \tag{A15}$$

The above equation shows that

$$\text{Proposition 3} \Longrightarrow \text{Proposition 2}. \tag{A16}$$

Proposition 2 $\Longrightarrow$ Proposition 3 can be shown as follows: Without loss of generality, $\rho_{X,A}^{\mathrm{GGE}}$ can be expressed as

$$\rho_{X,A}^{\mathrm{GGE}} = \frac{e^{-\mathcal{H}_A}}{\mathrm{Tr}_A(e^{-\mathcal{H}_A})}, \tag{A17}$$

where $\mathcal{H}_A$ is the entanglement Hamiltonian which is given by [138]

$$\mathcal{H}_A = \sum_{\mathbf{i},\mathbf{i}'\in A} K_{\mathbf{i},\mathbf{i}'}a_{\mathbf{i}}^\dagger a_{\mathbf{i}'}, \tag{A18}$$

with K being a $V_A \times V_A$ Hermitian matrix. Therefore, Proposition 2 is equivalent to stating that the entanglement Hamiltonian $\mathcal{H}_A$ is invariant under translations in the y direction, i.e.,

$$\text{Proposition 2} \Longleftrightarrow \mathcal{T}_A\mathcal{H}_A\mathcal{T}_A^{-1} = \mathcal{H}_A. \tag{A19}$$

This implies that we can decompose $\mathcal{H}_A$ in the transverse momentum sectors by taking the partial Fourier transform (12) in the y direction,

$$\mathcal{H}_A = \sum_{q_y}\sum_{i_x,i_x'=0}^{\ell-1} [K(q_y)]_{i_x,i_x'}c_{i_x,q_y}^\dagger c_{i_x',q_y}, \tag{A20}$$

where $K(q_y)$ is a $\ell \times \ell$ Hermitian matrix. On the other hand, if we express the matrix $U_A(t)$, defined in Eq. (124), in the mixed space-momentum basis,

$$U_A(t) = e^{-\mathrm{i}t\sum_{i_x=0}^{\ell-1}\sum_{q_y}\cos q_y c_{i_x,q_y}^\dagger c_{i_x,q_y}}, \tag{A21}$$

we find that

$$U_A(t)c_{i_x,q_y}U_A^\dagger(t) = c_{i_x,q_y}e^{-\mathrm{i}t\cos q_y}. \tag{A22}$$

Combining this result with Eq. (A20), we obtain

$$U_A(t)\mathcal{H}_A U_A^\dagger(t) = \mathcal{H}_A. \tag{A23}$$

Therefore, applying this identity in Eq. (A17),

$$U_A(t)\rho_{A,X}^{\mathrm{GGE}}U_A^\dagger(t) = \rho_{A,X}^{\mathrm{GGE}}. \tag{A24}$$

Thus, if we take the limit

$$\lim_{t\to\infty} \rho_A(t) = \lim_{t\to\infty} U_A(t)\rho_{X,A}(t)U_A^\dagger(t), \tag{A25}$$

we apply Assumption 1,

$$\lim_{t\to\infty} \rho_A(t) = \lim_{t\to\infty} U_A(t)\rho_{X,A}^{\mathrm{GGE}}U_A^\dagger(t), \tag{A26}$$

and Eq. (A24), we obtain

$$\lim_{t\to\infty} \rho_A(t) = \rho_{X,A}^{\mathrm{GGE}}. \tag{A27}$$

Equation (A27) shows that, if $\rho_{X,A}$ restores the transverse translational symmetry at large times, then $\rho_A(t)$ relaxes to a stationary state, i.e., Proposition 1 holds. Since we can use Assumption 2 when Proposition 1 holds, we can replace the left-hand side of Eq. (A27) with ρ_A^{GGE} and

$$\rho_A^{\mathrm{GGE}} = \rho_{X,A}^{\mathrm{GGE}}. \tag{A28}$$

Therefore, Proposition 2 $\Longrightarrow$ Proposition 3. This ends the proof of

$$\text{Proposition 2} \Longleftrightarrow \text{Proposition 3}. \tag{A29}$$

From (A9) and (A29), we have finally proved that

$$\text{Proposition 1} \Longleftrightarrow \text{Proposition 2}. \tag{A30}$$

APPENDIX B: PROOF OF THE CONDITION (128) FOR THE RESTORATION OF TRANSLATIONAL INVARIANCE IN THE *y* DIRECTION

In this Appendix, we show that $\rho_{X,A}(t)$ restores the translation symmetry in the y direction at large times, i.e., Proposition 2 is true, if and only if Eq. (128) is satisfied.

As mentioned in Appendix A, Proposition 2 is equivalent to saying that the stationary state $\lim_{t\to\infty}\rho_{A,X}(t) = \rho_{X,A}^{\mathrm{GGE}}$ is block diagonal in the q_y momentum sectors. Thus, we can verify whether Proposition 2 is satisfied or not by calculating the mixed space-momentum correlator

$$C_{i_x,i_x'}^{q_y,q_y'}(t) = \mathrm{Tr}_A(\rho_{X,A}(t) c_{i_x,q_y}^\dagger c_{i_x',q_y'}). \tag{B1}$$

Given Assumption 1, it is clear that $C_{i_x,i_x'}^{q_y,q_y'}(\infty) = 0\ \forall\ i_x, i_x' \in A, q_y \neq q_y'$ if and only if $\rho_{X,A}^{\mathrm{GGE}}$ is block diagonal in the q_y momentum sectors. Thus, in the following, we prove that $C_{i_x,i_x'}^{q_y,q_y'}(\infty) = 0$ if and only if Eq. (128) holds.

Using Assumption 1 and performing the Fourier transform in the x direction, we can rewrite $C_{i_x,i_x'}^{q_y,q_y'}(\infty)$ as

$$C_{i_x,i_x'}^{q_y,q_y'}(\infty) = \frac{1}{L_x}\sum_{q_x,q_x'} e^{-\mathrm{i}q_x i_x + \mathrm{i}q_x' i_x'} \mathrm{Tr}\big(\rho_X^{\mathrm{GGE}} \tilde{a}_{\mathbf{q}}^\dagger \tilde{a}_{\mathbf{q}'}\big). \tag{B2}$$

We recall that ρ_X^{GGE} is a GGE built with conserved charges of H^X, which is diagonalized as

$$H^X = \sum_{q_x}\sum_{i_y} \cos q_x d_{q_x,i_y}^\dagger d_{q_x,i_y} \tag{B3}$$

$$= \sum_{q_x}\sum_{\mu} \cos q_x \alpha_{q_x,\mu}^\dagger \alpha_{q_x,\mu}, \tag{B4}$$

where $\alpha_{q_x,\mu} = \sum_{i_y}[U(q_x)]_{\mu,i_y} d_{q_x,i_y}$ with $U(q_x)$ being a $L_y \times L_y$ unitary matrix. Therefore, without loss of generality, the conserved charges of H^X are given by $\hat{Q}_{q_x,\mu} = \alpha_{q_x,\mu}^\dagger \alpha_{q_x,\mu}$ and hence ρ_X^{GGE} can be written as

$$\rho_X^{\mathrm{GGE}} = \frac{e^{-\sum_{q_x,\mu}\lambda_{q_x,\mu}\hat{Q}_{q_x,\mu}}}{\mathrm{Tr}(e^{-\sum_{q_x,\mu}\lambda_{q_x,\mu}\hat{Q}_{q_x,\mu}})}. \tag{B5}$$

Even without knowing explicitly the form of $U(q_x)$, the previous equation shows that ρ_X^{GGE} has a block-diagonal form in the q_x momentum sectors. This implies that

$$\mathrm{Tr}\big(\rho_X^{\mathrm{GGE}} \tilde{a}_{\mathbf{q}}^\dagger \tilde{a}_{\mathbf{q}'}\big) = \delta_{q_x,q_x'} \mathrm{Tr}\big(\rho_X^{\mathrm{GGE}} \tilde{a}_{q_x,q_y}^\dagger \tilde{a}_{q_x,q_y'}\big). \tag{B6}$$

Plugging it into Eq. (B2), we obtain

$$C_{i_x,i_x'}^{q_y,q_y'}(\infty) = \frac{1}{L_x}\sum_{q_x} e^{-\mathrm{i}q_x(i_x - i_x')} \mathrm{Tr}\big(\rho_X^{\mathrm{GGE}} \tilde{a}_{q_x,q_y}^\dagger \tilde{a}_{q_x,q_y'}\big). \tag{B7}$$

Since the charges $\tilde{a}_{q_x,q_y}^\dagger \tilde{a}_{q_x,q_y'}$ are conserved by H^X,

$$\mathrm{Tr}\big(\rho_X^{\mathrm{GGE}} \tilde{a}_{q_x,q_y}^\dagger \tilde{a}_{q_x,q_y'}\big) = \langle\psi_0|\tilde{a}_{q_x,q_y}^\dagger \tilde{a}_{q_x,q_y'}|\psi_0\rangle \tag{B8}$$

and, substituting it into Eq. (B7), we arrive at

$$C_{i_x,i_x'}^{q_y,q_y'}(\infty) = \frac{1}{L_x}\sum_{q_x} e^{-\mathrm{i}q_x(i_x - i_x')} \langle\psi_0|\tilde{a}_{q_x,q_y}^\dagger \tilde{a}_{q_x,q_y'}|\psi_0\rangle. \tag{B9}$$

From this expression, we find that $C_{i_x,i_x'}^{q_y,q_y'}(\infty) = 0$ if and only if

$$\langle\psi_0|\tilde{a}_{q_x,q_y}^\dagger \tilde{a}_{q_x,q_y'}|\psi_0\rangle = 0\ \forall\ q_x, q_y \neq q_y'. \tag{B10}$$

APPENDIX C: INHOMOGENEOUS PARTIALLY FILLED PRODUCT STATE

In this Appendix, we analyze another example of a quench in which $\rho_A(t)$ does not relax to a stationary state, and thus the standard quasiparticle picture must be modified (see Sec. VI). Specifically, we consider the quantum quench from the inhomogeneous partially filled product state

$$|\mathrm{IPF}\rangle = \prod_{i_y=0}^{L_x-1} |\mathrm{IPF}\rangle_{i_y}, \tag{C1}$$

where $|\mathrm{IPF}\rangle_{i_y}$ is similar to the 1D cat state of Eq. (82) but now the angle θ that controls the occupation probability depends on the coordinate i_y,

$$|\mathrm{IPF}\rangle_{i_y} = \frac{1}{\sqrt{2+2(\cos\theta_{i_y})^{L_x}}}(|\theta_{i_y}\rangle - |-\theta_{i_y}\rangle). \tag{C2}$$

When $\theta_{i_y} = \theta$ for all i_y, $|\mathrm{IPF}\rangle$ is the the partially filled product state I discussed in Sec. IV G 1.

Evaluating the correlator of Eq. (128) in the state $|\mathrm{IPF}\rangle$, we have

$$\langle\mathrm{IPF}|\tilde{a}_{q_x,q_y}^\dagger \tilde{a}_{q_x,q_y'}|\mathrm{IPF}\rangle = \frac{1}{2L_y}\sum_{i_y} e^{\mathrm{i}(q_y - q_y')i_y}(1 - \cos\Delta_{q_x,i_y}), \tag{C3}$$

where $\cos\Delta_{q_x,i_y}$ is obtained by replacing θ in Eq. (88) with θ_{i_y}. If θ_{i_y} is independent of i_y, which corresponds to the case in Sec. IV G 1, this correlator vanishes for all q_x and $q_y \neq q_y'$. In that case, according to the results in Sec. VI B, $\rho_A(t)$ relaxes to a stationary state and the prediction of the standard quasiparticle picture (113) works. On the other hand, when θ_{i_y} depends on i_y, the correlator of Eq. (C3) is in general nonzero, and Eq. (128) is not satisfied. This implies that it does not exist a stationary state for $\rho_A(t)$.

When θ_{i_y} depends on i_y, the state $|\mathrm{IPF}\rangle$ has no translational symmetry in the y direction, hence, we cannot apply the dimensional reduction approach of Sec. III. Instead, when the initial state is the product state for each i_yth row as in Eq. (C1), we can calculate the Rényi entanglement entropy without using the dimensional reduction as follows. Let us decompose the time-evolution Hamiltonian as in Eq. (116). Since the operator $e^{-\mathrm{i}tH^X}$ has no dynamics in the y direction, it preserves the initial product structure for each i_yth row. Therefore, the reduced density matrix $\rho_{X,A}(t)$, introduced in Eq. (126), and obtained in this case from the state $e^{-\mathrm{i}tH^X}|\mathrm{IPF}\rangle$, is of the form

$$\rho_{X,A}(t) = \bigotimes_{i_y=0}^{L_y-1} \rho_{X,A,i_y}(t), \tag{C4}$$

where

$$\rho_{X,A,i_y}(t) = \mathrm{Tr}_{B,i_y}\left(e^{-\mathrm{i}tH^X_{i_y}}|\mathrm{IPF}\rangle_{i_y}\langle\mathrm{IPF}|e^{\mathrm{i}tH^X_{i_y}}\right), \tag{C5}$$

and Tr_{B,i_y} is the partial trace over the sites of the subsystem B in the i_yth row. Since $\rho_A(t)$ and $\rho_{X,A}(t)$ are related by the unitary transformation (125), we have $S_n(\rho_A(t)) = S_n(\rho_{X,A}(t))$. Therefore, if we further take into account that the Rényi entanglement entropy is additive in the tensor product,

$$S_n(\rho_A) = S_n(\rho_{X,A}) = \sum_{i_y=0}^{L_y-1} S_n(\rho_{X,A,i_y}). \tag{C6}$$

Since ρ_{X,A,i_y} is nothing but the reduced density matrix of the partially filled product state I of Sec. IV G 1 with $L_y = 1$, the asymptotic form of $S_n(\rho_{X,A,i_y})$ in the space-time scaling limit can be obtained by just setting $L_y = 1$ in Eq. (93). It reads as

$$S_n(\rho_{X,A,i_y}) \simeq \int_0^{2\pi} \frac{\mathrm{d}q_x}{2\pi} h_n(\cos\Delta_{q_x,i_y}) \min(\ell, 2t|v_x(q_x)|). \tag{C7}$$

Plugging the above equation into Eq. (C6) yields

$$S_n \simeq \sum_{i_y=0}^{L_y-1} \int_0^{2\pi} \frac{\mathrm{d}q_x}{2\pi} h_n(\cos\Delta_{q_x,i_y}) \min(\ell, 2t|v_x(q_x)|). \tag{C8}$$

Accordingly, the saturation value of the Rényi entanglement entropy is

$$\lim_{t\to\infty} S_n = \ell \sum_{i_y=0}^{L_y-1} \int_0^{2\pi} \frac{\mathrm{d}q_x}{2\pi} h_n(\cos\Delta_{q_x,i_y}). \tag{C9}$$

On the other hand, applying the standard quasiparticle picture of Sec. V to the state $|\mathrm{IPF}\rangle$, i.e., Eq. (113) with the expectation value of the conserved charges (C3), we find

$$S_n \simeq L_y \int_0^{2\pi} \frac{\mathrm{d}q_x}{2\pi} h_n\left(L_y^{-1}\sum_{i_y=0}^{L_y-1}\cos\Delta_{q_x,i_y}\right) \times \min(\ell, 2t|v_x(q_x)|). \tag{C10}$$

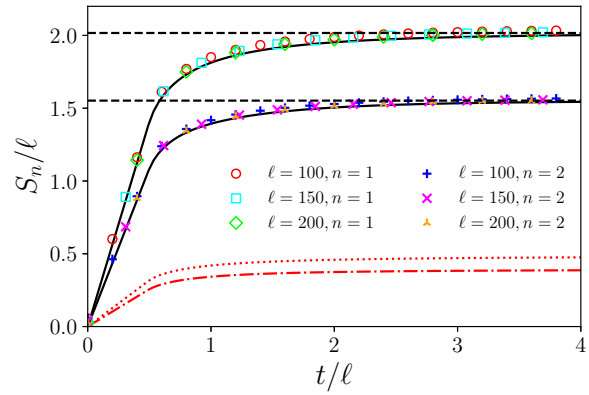

FIG. 11. Time evolution of the Rényi entanglement entropy after a quench from the inhomogeneous partially filled product state, taking as inhomogeneous angles $\theta_{i_y} = 2\pi i_y/L_y$ for the initial configuration and Rényi indices $n \to 1$ and $n = 2$. The solid lines correspond to the analytic prediction found in Eq. (C8). The symbols are the exact values of the entropy computed numerically with Eq. (8). The dashed lines are the large-time saturation value predicted in Eq. (C8). The dotted and dashed-dotted lines are the predictions of the standard quasiparticle picture in Eq. (C10) for $n \to 1$ and $n = 2$, respectively. In all cases, we take $L_y = 10$.

In Fig. 11, we plot as a function of time the Rényi entanglement entropies in the quench from the inhomogeneous partially filled product state with the inhomogeneous angle $\theta_{i_y} = 2\pi i_y/L_y$. The plot shows that the expression of Eq. (C8) (solid lines) agrees well with the exact values (symbols) of the entropies obtained by numerically with Eq. (8), whereas the prediction of the quasiparticle picture in Eq. (C10) (dashed curves) does not match the correct result.

This discrepancy means that, as in the case of the crossed dimer state, the entanglement entropies derived from the GGEs associated with H and H^X are different, and the correct one is the latter. In the present case, one finds that the GGE that reproduces the saturation value of the entanglement entropy in Eq. (C9) is built with the charges

$$\hat{n}_{q_x,i_y} = d^\dagger_{q_x,i_y} d_{q_x,i_y}, \tag{C11}$$

which commute with H^X but not with H.

Repeating the derivation of Eq. (110) for the current case, we find that the entropy of the GGE built with $\{\hat{n}_{q_x,i_y}\}$ is

$$S_n = \sum_{i_y=0}^{L_y-1} \int_0^{2\pi} \frac{\mathrm{d}q_x}{2\pi} h_n(2n_{q_x,i_y} - 1), \tag{C12}$$

where $n_{q_x,i_y} = \langle\psi_0|\hat{n}_{q_x,i_y}|\psi_0\rangle$. For the state $|\mathrm{IPF}\rangle$, this expectation value is

$$n_{q_x,i_y} = \frac{1-\cos\Delta_{q_x,i_y}}{2}. \tag{C13}$$

Plugging it into Eq. (C12), we indeed obtain Eq. (C9).

[1] A. Polkovnikov, K. Sengupta, A. Silva, and M. Vengalattore, Nonequilibrium dynamics of closed interacting quantum systems, Rev. Mod. Phys. **83**, 863 (2011).

[2] C. Gogolin and J. Eisert, Equilibration, thermalisation, and the emergence of statistical mechanics in closed quantum systems, Rep. Prog. Phys. **79**, 056001 (2016).

[3] P. Calabrese, F. H. L. Essler, and G. Mussardo, Introduction to quantum integrability in out of equilibrium systems, J. Stat. Mech. (2016) 064001.

[4] J. M. Deutsch, Quantum statistical mechanics in a closed system, Phys. Rev. A **43**, 2046 (1991).

[5] M. Srednicki, Chaos and quantum thermalization, Phys. Rev. E **50**, 888 (1994).

[6] H. Tasaki, From quantum dynamics to the canonical distribution: General picture and a rigorous Example, Phys. Rev. Lett. **80**, 1373 (1998).

[7] M. Rigol, V. Dunjko, and M. Olshanii, Thermalization and its mechanism for generic isolated quantum systems, Nature (London) **452**, 854 (2008).

[8] L. D'Alessio, Y. Kafri, A. Polkovnikov, and M. Rigol, From quantum chaos and eigenstate thermalization to statistical mechanics and thermodynamics, Adv. Phys. **65**, 239 (2016).

[9] M. Rigol, V. Dunjko, V. Yurovsky, and M. Olshanii, Relaxation in a completely integrable many-body quantum system: An ab initio study of the dynamics of the highly excited states of 1D lattice hard-core bosons, Phys. Rev. Lett. **98**, 050405 (2007).

[10] T. Barthel and U. Schollwock, Dephasing and the steady state in quantum many-particle systems, Phys. Rev. Lett. **100**, 100601 (2008).

[11] M. Cramer, C. M. Dawson, J. Eisert, and T. J. Osborne, Exact relaxation in a class of nonequilibrium quantum lattice systems, Phys. Rev. Lett. **100**, 030602 (2008).

[12] P. Calabrese, F. H. L. Essler, and M. Fagotti, Quantum quenches in the transverse field Ising chain: II. Stationary state properties, J. Stat. Mech. (2012) P07022.

[13] E. Ilievski, J. De Nardis, B. Wouters, J.-S. Caux, F. H. L. Essler, and T. Prosen, Complete generalized gibbs ensembles in an interacting theory, Phys. Rev. Lett. **115**, 157201 (2015).

[14] L. Vidmar and M. Rigol, Generalized Gibbs ensemble in integrable lattice models, J. Stat. Mech. (2016) 064007.

[15] F. H. L. Essler and M. Fagotti, Quench dynamics and relaxation in isolated integrable quantum spin chains J. Stat. Mech. (2016) 064002.

[16] L. Amico, R. Fazio, A. Osterloh, and V. Vedral, Entanglement in many-body systems, Rev. Mod. Phys. **80**, 517 (2008).

[17] P. Calabrese, J. Cardy, and B. Doyon, Entanglement entropy in extended quantum systems, J. Phys. A: Math. Theor. **42**, 500301 (2009).

[18] N. Laflorencie, Quantum entanglement in condensed matter systems, Phys. Rep. **646**, 1 (2016).

[19] T. Kinoshita, T. Wenger, and D. S. Weiss, A quantum Newton's cradle, Nature (London) **440**, 900 (2006).

[20] S. Hofferberth, I. Lesanovsky, B. Fischer, T. Schumm, and J. Schmiedmayer, Non-equilibrium coherence dynamics in one-dimensional Bose gases, Nature (London) **449**, 324 (2007).

[21] S. Trotzky, Y.-A. Chen, A. Flesch, I. P. McCulloch, U. Schollwöck, J. Eisert, and I. Bloch, Probing the relaxation towards equilibrium in an isolated strongly correlated one-dimensional Bose gas, Nat. Phys. **8**, 325 (2012).

[22] M. Gring, M. Kuhnert, T. Langen, T. Kitagawa, B. Rauer, M. Schreitl, I. Mazets, D. A. Smith, E. Demler, and J. Schmiedmayer, Relaxation and prethermalization in an isolated quantum system, Science **337**, 1318 (2012).

[23] M. Cheneau, P. Barmettler, D. Poletti, M. Endres, P. Schauß, T. Fukuhara, C. Gross, I. Bloch, C. Kollath, and S. Kuhr, Light-cone-like spreading of correlations in a quantum many-body system, Nature (London) **481**, 484 (2012).

[24] T. Langen, R. Geiger, M. Kuhnert, B. Rauer, and J. Schmiedmayer, Local emergence of thermal correlations in an isolated quantum many-body system, Nat. Phys. **9**, 640 (2013).

[25] F. Meinert, M. J. Mark, E. Kirilov, K. Lauber, P. Weinmann, A. J. Daley, and H.-C. Nägerl, Quantum quench in an atomic one-dimensional ising chain, Phys. Rev. Lett. **111**, 053003 (2013).

[26] T. Langen, S. Erne, R. Geiger, B. Rauer, T. Schweigler, M. Kuhnert, W. Rohringer, I. E. Mazets, T. Gasenzer, and J. Schmiedmayer, Experimental observation of a generalized Gibbs ensemble, Science **348**, 207 (2015).

[27] R. Islam, R. Ma, P. M. Preiss, M. Eric Tai, A. Lukin, M. Rispoli, and M. Greiner, Measuring entanglement entropy in a quantum many-body system, Nature (London) **528**, 77 (2015).

[28] A. M. Kaufman, M. E. Tai, A. Lukin, M. Rispoli, R. Schittko, P. M. Preiss, and M. Greiner, Quantum thermalization through entanglement in an isolated many-body system, Science **353**, 794 (2016).

[29] P. Calabrese and J. Cardy, Evolution of entanglement entropy in one-dimensional systems, J. Stat. Mech. (2005) P04010.

[30] J. M. Deutsch, H. Li, and A. Sharma, Microscopic origin of thermodynamic entropy in isolated systems, Phys. Rev. E **87**, 042135 (2013).

[31] V. Alba and P. Calabrese, Entanglement and thermodynamics after a quantum quench in integrable systems, Proc. Natl. Acad. Sci. USA **114**, 7947 (2017).

[32] M. Fagotti and P. Calabrese, Evolution of entanglement entropy following a quantum quench: Analytic results for the XY chain in a transverse magnetic field, Phys. Rev. A **78**, 010306(R) (2008).

[33] V. Eisler and I. Peschel, Entanglement in a periodic quench, Ann. Phys. **520**, 410 (2008).

[34] I. Peschel and V. Eisler, Reduced density matrices and entanglement entropy in free lattice models, J. Phys. A: Math. Theor. **42**, 504003 (2009).

[35] M. G. Nezhadhaghighi and M. A. Rajabpour, Entanglement dynamics in short- and long-range harmonic oscillators, Phys. Rev. B **90**, 205438 (2014).

[36] L. Bucciantini, M. Kormos, and P. Calabrese, Quantum quenches from excited states in the Ising chain, J. Phys. A: Math. Theor. **47**, 175002 (2014).

[37] A. S. Buyskikh, M. Fagotti, J. Schachenmayer, F. Essler, and A. J. Daley, Entanglement growth and correlation spreading with variable-range interactions in spin and fermionic tunneling models, Phys. Rev. A **93**, 053620 (2016).

[38] L. Hackl, E. Bianchi, R. Modak, and M. Rigol, Entanglement production in bosonic systems: Linear and logarithmic growth, Phys. Rev. A **97**, 032321 (2018).

[39] G. Del Vecchio Del Vecchio, B. Doyon, and P. Ruggiero, Entanglement Rényi entropies from ballistic fluctuation theory: The free fermionic case, SciPost Phys. Core **7**, 005 (2024).

[40] M. Collura, M. Kormos, and P. Calabrese, Stationary entanglement entropies following an interaction quench in 1D Bose gas, J. Stat. Mech. (2014) P01009.

[41] V. Alba and P. Calabrese, Entanglement dynamics after quantum quenches in generic integrable systems, SciPost Phys. **4**, 017 (2018).

[42] V. Alba and P. Calabrese, Quench action and Rényi entropies in integrable systems, Phys. Rev. B **96**, 115421 (2017).

[43] R. Modak, V. Alba, and P. Calabrese, Entanglement revivals as a probe of scrambling in finite quantum systems, J. Stat. Mech. (2020) 083110.

[44] R. Modak, L. Piroli, and P. Calabrese, Correlation and entanglement spreading in nested spin chains, J. Stat. Mech. (2019) 093106.

[45] K. Klobas and B. Bertini, Entanglement dynamics in Rule 54: Exact results and quasiparticle picture, SciPost Phys. **11**, 107 (2021).

[46] K. Klobas, B. Bertini, and L. Piroli, Exact thermalization dynamics in the "Rule 54" quantum cellular automaton, Phys. Rev. Lett. **126**, 160602 (2021).

[47] B. Bertini, M. Fagotti, L. Piroli, and P. Calabrese, Entanglement evolution and generalised hydrodynamics: Noninteracting systems, J. Phys. A: Math. Theor. **51**, 39LT01 (2018).

[48] C. Rylands and P. Calabrese, Transport and entanglement across integrable impurities from generalized hydrodynamics, Phys. Rev. Lett. **131**, 156303 (2023).

[49] V. Alba, B. Bertini, and M. FagottiEntanglement evolution and generalised hydrodynamics: Interacting integrable systems, SciPost Phys. **7**, 005 (2019).

[50] M. Mestyán and V. Alba, Molecular dynamics simulation of entanglement spreading in generalized hydrodynamics, SciPost Phys. **8**, 055 (2020).

[51] B. Bertini, E. Tartaglia, and P. Calabrese, Entanglement and diagonal entropies after a quench with no pair structure, J. Stat. Mech. (2018) 063104.

[52] X. Cao, A. Tilloy, and A. De Luca, Entanglement in a fermion chain under continuous monitoring, SciPost Phys. **7**, 024 (2019).

[53] A. Bastianello and P. Calabrese, Spreading of entanglement and correlations after a quench with intertwined quasiparticles, SciPost Phys. **5**, 033 (2018).

[54] A. Bastianello and M. Collura, Entanglement spreading and quasiparticle picture beyond the pair structure, SciPost Phys. **8**, 045 (2020).

[55] V. Alba and F. Carollo, Spreading of correlations in Markovian open quantum systems, Phys. Rev. B **103**, L020302 (2021).

[56] F. Carollo and V. Alba, Entangled multiplets and unusual spreading of quantum correlations in a continuously monitored tight-binding chain, Phys. Rev. B **106**, L220304 (2022).

[57] B. Bertini and P. Calabrese, Prethermalization and thermalization in entanglement dynamics, Phys. Rev. B **102**, 094303 (2020).

[58] F. Carollo and V. Alba, Dissipative quasiparticle picture for quadratic Markovian open quantum systems, Phys. Rev. B **105**, 144305 (2022).

[59] V. Alba and F. Carollo, Hydrodynamics of quantum entropies in Ising chains with linear dissipation, J. Phys. A: Math. Theor. **55**, 074002 (2022).

[60] S. Chapman, J. Eisert, L. Hackl, M. P. Heller, R. Jefferson, H. Marrochio, and R. C. Myers, Complexity and entanglement for thermofield double states, SciPost Phys. **6**, 034 (2019).

[61] G. Lagnese, P. Calabrese, and L. Piroli, Entanglement dynamics of thermofield double states in integrable models, J. Phys. A: Math. Theor. **55**, 214003 (2022).

[62] X. Turkeshi and M. Schiró, Entanglement and correlation spreading in non-Hermitian spin chains, Phys. Rev. B **107**, L020403 (2023).

[63] D. X. Horvath, P. Calabrese, and O. A. Castro-Alvaredo, Entanglement of stationary states in the presence of unstable quasiparticles, J. High Energy Phys. 04 (2023) 091.

[64] M. Gruber and V. Eisler, Magnetization and entanglement after a geometric quench in the XXZ chain, Phys. Rev. B **99**, 174403 (2019).

[65] S. Fraenkel and M. Goldstein, Extensive long-range entanglement in a nonequilibrium steady state, SciPost Phys. **15**, 134 (2023).

[66] L. Capizzi, S. Scopa, F. Rottoli, and P. Calabrese, Domain wall melting across a defect, Europhys. Lett. **141**, 31002 (2023).

[67] D. Kagamihara, R. Kaneko, S. Yamashika, K. Sugiyama, R. Yoshii, S. Tsuchiya, and I. Danshita, Rényi entanglement entropy after a quantum quench starting from insulating states in a free boson system, Phys. Rev. A **107**, 033305 (2023).

[68] S. Yamashika, D. Kagamihara, R. Yoshii, and S. Tsuchiya, Evolution of entanglement entropy in strongly correlated bosons in an optical lattice, Phys. Rev. Res. **5**, 043102 (2023).

[69] P. Calabrese and J. Cardy, Time-dependence of correlation functions following a quantum quench, Phys. Rev. Lett. **96**, 136801 (2006).

[70] V. Alba and P. Calabrese, Quantum information scrambling after a quantum quench, Phys. Rev. B **100**, 115150 (2019).

[71] V. Alba and P. Calabrese, Quantum information dynamics in multipartite integrable systems, Europhys. Lett. **126**, 60001 (2019).

[72] A. Coser, E. Tonni, and P. Calabrese, Entanglement negativity after a global quantum quench, J. Stat. Mech. (2014) P12017.

[73] S. Murciano, V. Alba, and P. Calabrese, Quench Dynamics of Rényi Negativities and the Quasiparticle Picture, in *Entanglement in Spin Chains*, edited by A. Bayat, S. Bose, and H. Johannesson (Springer, Berlin, 2022), p. 397.

[74] G. Parez, R. Bonsignori, and P. Calabrese, Dynamics of charge-imbalance-resolved entanglement negativity after a quench in a free-fermion model, J. Stat. Mech. (2022) 053103.

[75] B. Bertini, K. Klobas, and T.-C. Lu, Entanglement negativity and mutual information after a quantum Quench: Exact link from space-time duality, Phys. Rev. Lett. **129**, 140503 (2022).

[76] J. Dubail, Entanglement scaling of operators: A conformal field theory approach, with a glimpse of simulability of long-time dynamics in 1+1d, J. Phys. A: Math. Theor. **50**, 234001 (2017).

[77] A. Lerose, M. Sonner, and D. A. Abanin, Scaling of temporal entanglement in proximity to integrability, Phys. Rev. B **104**, 035137 (2021).

[78] G. Giudice, G. Giudici, M. Sonner, J. Thoenniss, A. Lerose, D. A. Abanin, and L. Piroli, Temporal entanglement, quasiparticles, and the role of interactions Phys. Rev. Lett. **128**, 220401 (2022).

[79] G. Parez, R. Bonsignori, and P. Calabrese, Quasiparticle dynamics of symmetry resolved entanglement after a quench:

The examples of conformal field theories and free fermions, Phys. Rev. B **103**, L041104 (2021).
[80] G. Parez, R. Bonsignori, and P. Calabrese, Exact quench dynamics of symmetry resolved entanglement in a free fermion chain, J. Stat. Mech. (2021) 093102.
[81] L. Piroli, E. Vernier, M. Collura, and P. Calabrese, Thermodynamic symmetry resolved entanglement entropies in integrable systems, J. Stat. Mech. (2022) 073102.
[82] B. Bertini, P. Calabrese, M. Collura, K. Klobas, and C. Rylands, Nonequilibrium full counting statistics and symmetry-resolved entanglement from space-time duality, Phys. Rev. Lett. **131**, 140401 (2023).
[83] B. Bertini, K. Klobas, M. Collura, P. Calabrese, and C. Rylands, Dynamics of charge fluctuations from asymmetric initial states, arXiv:2306.12404.
[84] J. Kudler-Flam, Y. Kusuki, and S. Ryu, Correlation measures and the entanglement wedge cross-section after quantum quenches in two-dimensional conformal field theories, J. High Energy Phys. 04 (2020) 074.
[85] S. Murciano, V. Alba, and P. Calabrese, Symmetry-resolved entanglement in fermionic systems with dissipation, J. Stat. Mech. (2023) 113102.
[86] B. Bertini, K. Klobas, V. Alba, G. Lagnese, and P. CalabreseGrowth of rényi entropies in interacting integrable models and the breakdown of the quasiparticle picture, Phys. Rev. X **12**, 031016 (2022).
[87] S. Gopalakrishnan, D. A. Huse, V. Khemani, and R. Vasseur, Hydrodynamics of operator spreading and quasiparticle diffusion in interacting integrable systems, Phys. Rev. B **98**, 220303(R) (2018).
[88] F. Ares, S. Murciano, and P. Calabrese, Entanglement asymmetry as a probe of symmetry breaking, Nat. Commun. **14**, 2036 (2023).
[89] F. Ares, S. Murciano, E. Vernier, and P. Calabrese, Lack of symmetry restoration after a quantum quench: An entanglement asymmetry study, SciPost Phys. **15**, 089 (2023).
[90] C. Rylands, K. Klobas, F. Ares, P. Calabrese, S. Murciano, and B. Bertini, Microscopic origin of the quantum Mpemba effect in integrable systems, arXiv:2310.04419.
[91] S. Murciano, F. Ares, I. Klich, and P. Calabrese, Entanglement asymmetry and quantum Mpemba effect in the XY spin chain, J. Stat. Mech. (2024) 013103.
[92] F. Caceffo and V. Alba, Negative tripartite information after quantum quenches in integrable systems, Phys. Rev. B **108**, 134434 (2023).
[93] P. Calabrese, Entanglement and thermodynamics in non-equilibrium isolated quantum systems, Phys. A (Amsterdam) **504**, 31 (2018).
[94] P. Calabrese, Entanglement spreading in non-equilibrium integrable systems, SciPost Phys. Lect. Notes 20 (2020).
[95] A. Laeuchli and C. Kollath, Spreading of correlations and entanglement after a quench in the one-dimensional Bose-Hubbard model, J. Stat. Mech. (2008) P05018.
[96] H. Kim and D. A. Huse, Ballistic spreading of entanglement in a diffusive nonintegrable system, Phys. Rev. Lett. **111**, 127205 (2013).
[97] R. Pal and A. Lakshminarayan, Entangling power of time-evolution operators in integrable and nonintegrable many-body systems, Phys. Rev. B **98**, 174304 (2018).
[98] B. Bertini, P. Kos, and T. Prosen, Entanglement spreading in a minimal model of maximal many-body quantum chaos, Phys. Rev. X **9**, 021033 (2019).
[99] L. Piroli, B. Bertini, J. I. Cirac, and T. Prosen, Exact dynamics in dual-unitary quantum circuits, Phys. Rev. B **101**, 094304 (2020).
[100] A. Nahum, J. Ruhman, S. Vijay, and J. Haah, Quantum entanglement growth under random unitary dynamics, Phys. Rev. X **7**, 031016 (2017).
[101] T. Zhou and A. Nahum, Entanglement membrane in chaotic many-body systems, Phys. Rev. X **10**, 031066 (2020).
[102] S. Murciano, P. Calabrese, and R. M. Konik, Post-quantum quench growth of renyi entropies in low dimensional continuum bosonic systems, Phys. Rev. Lett. **129**, 106802 (2022).
[103] C. Holzhey, F. Larsen, and F. Wilczek, Geometric and renormalized entropy in conformal field theory, Nucl. Phys. B **424**, 443 (1994).
[104] P. Calabrese and J. Cardy, Entanglement entropy and quantum field theory, J. Stat. Mech. (2004) P06002.
[105] A. Lukin, M. Rispoli, R. Schittko, M. E. Tai, A. M. Kaufman, S. Choi, V. Khemani, J. Léonard, and M. Greiner, Probing entanglement in a many-body-localized system, Science **364**, 256 (2019).
[106] T. Brydges, A. Elben, P. Jurcevic, B. Vermersch, C. Maier, B. P. Lanyon, P. Zoller, R. Blatt, and C. F. Roos, Probing entanglement entropy via randomized measure-ments, Science **364**, 260 (2019).
[107] A. Elben, R. Kueng, H. Y. R. Huang, R. van Bij-nen, C. Kokail, M. Dalmonte, P. Calabrese, B. Kraus, J. Preskill, P. Zoller, and B. Vermersch, Mixed-state entanglement from local randomized measurements, Phys. Rev. Lett. **125**, 200501 (2020).
[108] A. Neven, J. Carrasco, V. Vitale, C. Kokail, A. Elben, M. Dalmonte, P. Calabrese, P. Zoller, B. Vermersch, R. Kueng, and B. Kraus, Symmetry-resolved entanglement detection using partial transpose moments, npj Quantum Inf. **7**, 152 (2021).
[109] V. Vitale, A. Elben, R. Kueng, A. Neven, J. Carrasco, B. Kraus, P. Zoller, P. Calabrese, B. Vermersch, and M. Dalmonte, Symmetry-resolved dynamical purification in synthetic quantum matter, SciPost Phys. **12**, 106 (2022).
[110] A. Rath, V. Vitale, S. Murciano, M. Votto, J. Dubail, R. Kueng, C. Branciard, P. Calabrese, and B. Vermersch, Entanglement barrier and its symmetry resolution: Theory and experiment, PRX Quantum **4**, 010318 (2023).
[111] J. Eisert, M. Cramer, and M. B. Plenio, Area laws for the entanglement entropy, Rev. Mod. Phys. **82**, 277 (2010).
[112] M. B. Plenio, J. Eisert, J. Dreissig, and M. Cramer, Entropy, entanglement, and area: Analytical results for harmonic lattice systems, Phys. Rev. Lett. **94**, 060503 (2005).
[113] D. Gioev and I. Klich, Entanglement entropy of fermions in any dimension and the widom conjecture, Phys. Rev. Lett. **96**, 100503 (2006).
[114] M. M. Wolf, Violation of the entropic area law for fermions, Phys. Rev. Lett. **96**, 010404 (2006).
[115] W. Li, L. Ding, R. Yu, T. Roscilde, and S. Haas, Scaling behavior of entanglement in two- and three-dimensional free fermions, Phys. Rev. B **74**, 073103 (2006).
[116] T. Barthel, M.-C. Chung, and U. Schollwöck, Entanglement scaling in critical two-dimensional fermionic and bosonic systems, Phys. Rev. A **74**, 022329 (2006).

[117] M. Cramer, J. Eisert, M. B. Plenio, and J. Dreissig, An entanglement-area law for general bosonic harmonic lattice systems, Phys. Rev. A **73**, 012309 (2006).
[118] H. Casini and M. Huerta, Universal terms for the entanglement entropy in 2+1 dimensions, Nucl. Phys. B **764**, 183 (2007).
[119] S. Farkas and Z. Zimboras, The von Neumann entropy asymptotics in multidimensional fermionic systems, J. Math. Phys. **48**, 102110 (2007).
[120] R. Helling, H. Leschke, and W. L. Spitzer, A special case of conjecture by Widom with implications to fermionic entanglement entropy, Int. Math. Res. Not. **2011**, 1451 (2011).
[121] A. J. A. James and R. M. Konik, Understanding the entanglement entropy and spectra of 2D quantum systems through arrays of coupled 1D chains, Phys. Rev. B **87**, 241103(R) (2013).
[122] P. Calabrese, M. Mintchev, and E. Vicari, Entanglement entropies in free fermion gases for arbitrary dimension, Europhys. Lett. **97**, 20009 (2012).
[123] J. Cardy, Some results on mutual information of disjoint regions in higher dimensions, J. Phys. A: Math. Theor. **46**, 285402 (2013).
[124] B. Swingle, Renyi entropy, mutual information, and fluctuation properties of Fermi liquids, Phys. Rev. B **86**, 045109 (2012).
[125] P. Calabrese, M. Mintchev, and E. Vicari, Exact relations between particle fluctuations and entanglement in Fermi gases, Europhys. Lett. **98**, 20003 (2012).
[126] F. Ares, J. G. Esteve, F. Falceto, and E. Sánchez-Burillo, Excited state entanglement in homogeneous fermionic chains, J. Phys. A: Math. Theor. **47**, 245301 (2014).
[127] I. Frérot and T. Roscilde, Area law and its violation: A microscopic inspection into the structure of entanglement and fluctuations, Phys. Rev. B **92**, 115129 (2015).
[128] M. T. Tan and S. Ryu, Rényi and symmetry-resolved entanglement entropy in two-dimensional fermi gas from multi-dimensional bosonization, Phys. Rev. B **101**, 235169 (2020).
[129] S. Murciano, P. Ruggiero, and P. Calabrese, Symmetry resolved entanglement in two-dimensional systems via dimensional reduction, J. Stat. Mech. (2020) 083102.
[130] S. Fraenkel and M. Goldstein, Symmetry resolved entanglement: Exact results in 1D and beyond, J. Stat. Mech. (2020) 033106.
[131] M. Nozaki, T. Numasawa, and T. Takayanagi, Quantum entanglement of local operators in conformal field theories, Phys. Rev. Lett. **112**, 111602 (2014).
[132] H. Casini, H. Liu, and M. Mezei, Spread of entanglement and causality, J. High Energy Phys. 07 (2016) 077.
[133] M. Mezei, On entanglement spreading from holography, J. High Energy Phys. 05 (2017) 064.
[134] J. S. Cotler, M. P. Hertzberg, M. Mezei, and M. T. Mueller, Entanglement growth after a global quench in free scalar field theory, J. High Energy Phys. 11 (2016) 166.
[135] M. Mezei and W. van der Schee, Black holes often saturate entanglement entropy the fastest, Phys. Rev. Lett. **124**, 201601 (2020).
[136] Y. Lemonik and A. Mitra, Entanglement properties of the critical quench of O(N) bosons, Phys. Rev. B **94**, 024306 (2016).
[137] M. C. Chung and I. Peschel, Density-matrix spectra for two-dimensional quantum systems, Phys. Rev. B **62**, 4191 (2000).
[138] I. Peschel, Calculation of reduced density matrices from correlation functions, J. Phys. A: Math. Gen. **36**, L205 (2003).
[139] P. Calabrese, F. H. L. Essler, and M. Fagotti, Quantum quench in the transverse field Ising chain: I. Time evolution of order parameter correlators, J. Stat. Mech. (2012) P07016.
[140] M. Fagotti and F. H. L. Essler, Reduced density matrix after a quantum quench, Phys. Rev. B **87**, 245107 (2013).
[141] M. Fagotti, On conservation laws, relaxation and pre-relaxation after a quantum quench, J. Stat. Mech. (2014) P03016.
[142] S. Groha, F. H. L. Essler, and P. Calabrese, Full counting statistics in the transverse field ising chain, SciPost Phys. **4**, 043 (2018).
[143] F. Ferro, F. Ares, and P. Calabrese, Non-equilibrium entanglement asymmetry for discrete groups: The example of the XY spin chain, J. Stat. Mech. (2024) 023101.
[144] E. B. Mpemba and D. G. Osborne, Cool? Phys. Educ. **4**, 172 (1969).
[145] Z. Lu and O. Raz, Nonequilibrium thermodynamics of the Markovian Mpemba effect and its inverse, Proc. Natl. Acad. Sci. USA **114**, 5083 (2017).
[146] I. Klich, O. Raz, O. Hirschberg, and M. Vucelja, Mpemba index and anomalous relaxation, Phys. Rev. X **9**, 021060 (2019).
[147] A. Kumar and J. Bechhoefer, Exponentially faster cooling in a colloidal system, Nature (London) **584**, 64 (2020).
[148] M. Gibbins, A. Jafarizadeh, A. Smith, and B. Bertini, Quench dynamics in lattices above one dimension: The free fermionic case, arXiv:2310.18227.